

Exploring Robustness of Bistability in Prototypical Positive Feedback Loops

Inauguraldissertation
zur
Erlangung der Würde eines Doktors der Philosophie
vorgelegt der
Philosophisch-Naturwissenschaftlichen Fakultät
der Universität Basel

von

Amirhossein Hajihosseini
aus Tehran, Iran

Basel, 2015

Originaldokument gespeichert auf dem Dokumentenserver der Universität Basel
edoc.unibas.ch



This work is licenced under the agreement
Attribution Non-Commercial No Derivatives - 3.0 Switzerland (CC BY-NC-ND 3.0 CH).

The complete text may be reviewed here:
creativecommons.org/licenses/by-nc-nd/3.0/ch/deed.en

Genehmigt von der Philosophisch-Naturwissenschaftlichen Fakultät
auf Antrag von

Prof. Attila Becskei und Prof. Ruedi Stoop

Basel, den 8. Dezember 2015

Prof. Dr. Jörg Schibler

Dekan



Namensnennung-Keine kommerzielle Nutzung-Keine Bearbeitung 3.0
Schweiz
(CC BY-NC-ND 3.0 CH)

Sie dürfen: **Teilen** - den Inhalt kopieren, verbreiten und zugänglich machen

Unter den folgenden Bedingungen:



Namensnennung – Sie müssen den Namen des Autors/Rechteinhabers in der von ihm festgelegten Weise nennen.



Keine kommerzielle Nutzung – Sie dürfen diesen Inhalt nicht für kommerzielle Zwecke nutzen.



Keine Bearbeitung erlaubt – Sie dürfen diesen Inhalt nicht bearbeiten, abwandeln oder in anderer Weise verändern.

Wobei gilt:

- **Verzichtserklärung** – Jede der vorgenannten Bedingungen kann **aufgehoben** werden, sofern Sie die ausdrückliche Einwilligung des Rechteinhabers dazu erhalten.
- **Public Domain (gemeinfreie oder nicht-schützbarer Inhalte)** – Soweit das Werk, der Inhalt oder irgendein Teil davon zur Public Domain der jeweiligen Rechtsordnung gehört, wird dieser Status von der Lizenz in keiner Weise berührt.
- **Sonstige Rechte** – Die Lizenz hat keinerlei Einfluss auf die folgenden Rechte:
 - Die Rechte, die jedermann wegen der Schranken des Urheberrechts oder aufgrund gesetzlicher Erlaubnisse zustehen (in einigen Ländern als grundsätzliche Doktrin des **fair use** bekannt);
 - Die **Persönlichkeitsrechte** des Urhebers;
 - Rechte anderer Personen, entweder am Lizenzgegenstand selber oder bezüglich seiner Verwendung, zum Beispiel für **Werbung** oder Privatsphärenschutz.
- **Hinweis** – Bei jeder Nutzung oder Verbreitung müssen Sie anderen alle Lizenzbedingungen mitteilen, die für diesen Inhalt gelten. Am einfachsten ist es, an entsprechender Stelle einen Link auf diese Seite einzubinden.

Quelle: <http://creativecommons.org/licenses/by-nc-nd/3.0/ch/> Datum: 12.11.2013

To the love of my life

Farzaneh

Abstract

Bistability is a dynamical property of biological systems which have the ability to possess two distinct stable steady states. Bistability is the hallmark of decision-making processes and underlies basic cellular functions such as cell cycle progression, cellular differentiation, and apoptosis. It is crucial for a bistable system to operate robustly, meaning that it has to be able to maintain the bistable behavior in the presence of perturbations in its kinetic parameters. We aim to understand how different parameter configurations and ultrasensitive mechanisms such as molecular cooperativity, homodimerization and titration, organize bistability and its robustness in prototypical feedback loop systems. We in particular show that the coupling between a positive and a negative feedback loop, enclosed under the titration mechanism, can enlarge the bistability range of a single parameter, and therefore contribute to the robustness of bistability. We also develop a method based on the open-loop approach to explore parametric regions inside the bistability area of bifurcation diagrams, in which the sensitivity of unstable steady state to parameters of a system can be minimized. Unstable steady states are key organizers of bistability and minimization of their sensitivity to parameters leads to the persistence of the bistable behavior against parameter perturbations. Our results provide insight into the role of different parameters as well as homodimerization and titration mechanisms in creating robust bistability in positive feedback systems. Additionally, we study the galactose network in *Saccharomyces cerevisiae*, in which bistability creates a persistent memory of the carbon source that is available in the environment. We reconstruct the bistable behavior of the network by developing a mathematical model that represents the molecular interactions of the network. Using the experimental data extracted from different layers of the network, we perform nonlinear regression to estimate the parameter values of the model. Our investigations reveal the significance of homodimerization and titration in creating bistability in the galactose network. In summary, our results provide a better understanding of how parameter configurations and different ultrasensitive regulatory motifs contribute to bistability and its robustness. The results can be used to efficiently design and synthesize robust bistable switches.

Contents

| | |
|---|-----------|
| Contents | v |
| 1 Introduction | 1 |
| 1.1 Dynamical systems | 2 |
| 1.2 Hill function and molecular cooperativity: The concept of ultra-sensitivity | 2 |
| 1.3 Biological feedback loops | 3 |
| 1.4 Positive feedback loops and bistability | 4 |
| 1.5 Robustness | 7 |
| 1.5.1 Bifurcation theory | 8 |
| 1.5.1.1 Saddle-node (fold) bifurcation | 9 |
| 1.5.1.2 Cusp bifurcation | 10 |
| 1.5.2 Parametric sensitivity analysis | 11 |
| 1.6 The open-loop approach: The concept of loop opening in biological feedback systems | 11 |
| 1.6.1 The self-activating system | 12 |
| 1.6.1.1 The closed-loop system | 12 |
| 1.6.1.2 The open-loop system | 13 |
| 2 Results | 16 |
| 2.1 Exploring the extrema of the bistability range of a single parameter | 17 |
| 2.2 Exploring robust regions of the bistability area | 26 |
| 2.2.1 The closed-loop sensitivity analysis: The unstable steady state sensitivity to parameters | 29 |
| 2.2.2 Formulation of the robustness analysis method based on the open-loop sensitivity | 31 |
| 2.2.3 One-gene positive feedback loop with protein homodimerization | 35 |
| 2.2.4 One-gene positive feedback loop with molecular titration . | 41 |
| 2.3 The <i>GAL</i> network | 47 |

| | | |
|----------|--|-----------|
| 2.3.1 | The 1 st layer of the galactose network: Gal4p decay data | 48 |
| 2.3.1.1 | Gal4p decay process in galactose | 48 |
| 2.3.1.2 | The regulatory effect of Gal4p protein on the <i>GAL7/GCY1</i> promoter response | 50 |
| 2.3.2 | The 2 nd layer of the galactose network: Gal80p decay data | 59 |
| 2.3.2.1 | Gal80p protein decay process in galactose | 60 |
| 2.3.2.2 | The regulatory effect of Gal80p protein on the <i>GAL7/GCY1</i> promoter response | 61 |
| 2.3.3 | The third layer of the galactose network: Opening the <i>GAL1</i> feedback loop | 65 |
| 3 | Conclusions | 69 |
| 3.1 | Extrema in the bistability range of a single parameter | 70 |
| 3.2 | Robust regions in the bistability area | 71 |
| 3.3 | Bistability in the <i>GAL</i> network | 71 |
| | Bibliography | 75 |

Chapter 1

Introduction

Systems biology is defined as a discipline that employs mathematical models to investigate molecular interactions and the specific phenotype which results from such interactions [2, 41, 83]. In the late 1950's and early 1960's, significant contributions were made to the field of systems biology thanks to a series of discoveries such as the existence of feedback control loops in gene expression [39, 91], bistability in *lac* operon [62] and oscillations in yeast glycolysis [27]. Later in the early 1970's, detailed studies on Belousov-Zhabotinsky chemical reactions [22, 23] provided yet another example of important contributions of mathematical modeling to the field. Based on these seminal studies, many biologist [24, 32, 63, 92] were already convinced by the late 1990's and early 2000's that the need for rigorous mathematical modeling of biological systems and interactions is undeniable. In the early 21st century, systems biology witnessed another incredible step forward as artificial genetic networks were synthesized. In particular, Gardner et al. [25] designed a synthetic toggle switch and Elowitz et al. [21] built an artificial oscillator with three repressing genes. These and other synthetic biological networks [11, 12] gave birth to a new field called synthetic biology [33].

Many mathematical models in systems biology, termed as mechanistic models, are defined by dynamical systems. Lotka [50] and Volterra [96] were among the very first theoretical biologists who considered biological systems as dynamical systems. The main idea behind using dynamical systems to model biological systems is to mathematically represent different cellular states as attractors of the system. In 1975, Waddington [97] put forth the idea of epigenetic landscape to illustrate different cellular states as attractors which in turn define cellular decisions. The emergence of such attractors are dependent on the number and type of interactions among different elements of the biological network.

1.1 Dynamical systems

Dynamical systems [31, 67, 98] are sets of differential equations that describe changes of physical quantities through the time. In biological systems, these quantities are mainly concentrations of chemical species. In gene regulatory networks in particular, one is interested to investigate variations in the concentration of mRNAs and proteins. Mathematically speaking, a dynamical system is represented as a system of first order ordinary differential equations

$$\dot{X}(t) = \frac{dX(t)}{dt} = F(X(t), \Theta), \quad (1.1)$$

where $X = (x_1, x_2, \dots, x_n) \in \mathbb{R}^n$ is a vector of state variables that changes with time, $\Theta \in \mathbb{R}^n$ is the vector of all parameters, and $F = (f_1, f_2, \dots, f_n) \in \mathbb{R}^n$ is the vector field. System (1.1) is called a parameter-dependent dynamical system. Solutions of system (1.1) are called trajectories of the system. The values of state variables for which the vector field vanishes are called the steady states of the system. The stable steady states absorb all nearby trajectories, while the unstable steady states repel the trajectories of the system.

1.2 Hill function and molecular cooperativity: The concept of ultrasensitivity

Hemoglobin is a protein in the red blood cells that facilitates the transportation of oxygen from respiratory system to the tissues. Under high pressure in the lungs, oxygen has a very high affinity to hemoglobin, while in the tissues the affinity is very low so that the oxygen dissociates from the hemoglobin. Investigations on hemoglobin and its interaction with oxygen was first done in early twentieth century by Hill [34] and Pauling [66]. In order to describe the experimental data for the binding of oxygen to hemoglobin which had a sigmoidal shape, Hill used the following function

$$y = \frac{x^n}{K^n + x^n}. \quad (1.2)$$

Equation (1.2) is called the Hill function and represents the fraction of occupancy of hemoglobin by oxygen. Later in mid twentieth century, it became possible to provide an explanation for equation (1.2) thanks to the works of Monod and his colleagues [55, 56, 57] on enzymatic reactions. For the binding of oxygen to hemoglobin, Monod et al. [56] proposed the allosteric theory to explain the cooperative behavior of hemoglobin proteins. According to this theory,

the binding of a ligand to a binding site alters the affinity of the ligand to other binding sites. This phenomenon is called positive cooperativity. Figure (1.1) shows that for $n > 1$, equation (1.2) is a sigmoidal function. As the value of n

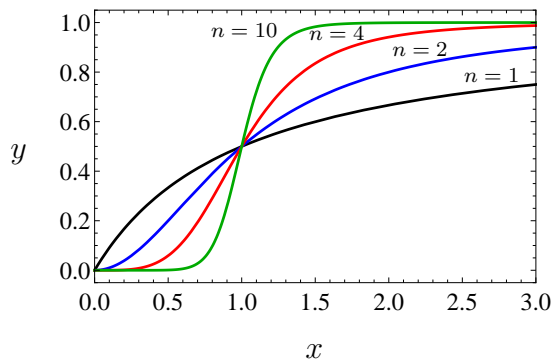


Figure 1.1: Graph of Hill function (1.2) for $K = 1$ and different values of the Hill number n . For $n > 1$, the curve is sigmoidal and exhibits ultrasensitivity because of the cooperativity phenomenon.

increases, the curve becomes steeper. A sigmoidal curve represents a very important characteristic of every biological switch which is called ultrasensitivity. Ultrasensitivity means that small fold changes in the input to a system can lead to large fold changes in the response. In Figure (1.1), for $n = 1$, y exhibits a graded variation as x changes, while for $n > 1$, there will be a binary change in the value of y since after a certain threshold, further variations in x lead to an abrupt change in the value of y .

Molecular cooperativity is not the only source of ultrasensitivity in biochemical and signaling networks. There are other well-known motifs whose presence can create ultrasensitivity. They include homo- and hetero-multimerization, multistep signaling and zero-order ultrasensitivity; the interested reader is referred to [100] for a complete review of the mentioned motifs. We will address in detail homodimerization and molecular titration (heterodimerization) in the next chapter as we study systems which consist of positive feedback loops and these two mechanisms.

1.3 Biological feedback loops

The notion of feedback can be defined in control systems as the capability of the system to use its output as its input to monitor a process that is controlled based on a specific property [40, 64]. In biological systems which are represented

by a dynamical system, feedback loops or circuits are defined as entries of the Jacobian matrix of the dynamical system [68, 85, 86]. For a dynamical system defined by equation (1.1), entries of the Jacobian matrix are given by

$$J_{ij} = \frac{\partial f_i}{\partial x_j}, \quad i, j = 1, 2, \dots, n. \quad (1.3)$$

If $J_{i,j} \neq 0$, changes in the j^{th} variable x_j affect the time evolution f_i of the i^{th} variable x_i . Based on the above definition, one can easily plot the directed graph of the system in which the nodes represent biological components or concentrations and the edges determine whether two nodes interact with each other if $J_{i,j}$ in equation (1.3) is not zero. Moreover, depending on the sign of $J_{i,j}$, the interaction can be positive or negative, meaning that the interacting biological components can activate or inhibit each other's activity. A loop or circuit is determined by a sequence of Jacobian matrix entries whose i and j indices define circular permutations [86]. The sign of a loop is given as the multiplication of the sign of individual interactions in the loop. Therefore, a feedback loop is positive if either all the interactions are positive or the number of negative interactions is even. Likewise, a feedback loop is negative if it has an odd number of negative interactions. Figure (1.2) illustrates three simple examples of two-node and three-node positive and negative feedback loops: a double-positive and a double-negative feedback loop which are both positive feedback loops plus a three-node negative feedback loop. The positive interactions are denoted by " \rightarrow " and the negative interactions are shown by " \dashv ".

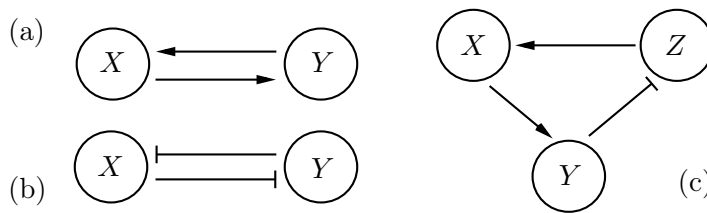


Figure 1.2: Positive and negative feedback loops. (a) A positive feedback loop with two positive interactions. (b) A positive feedback loop in which the two components negatively regulate each other. (c) A negative feedback loop with one negative and two positive interactions.

1.4 Positive feedback loops and bistability

It was first conjectured by Thomas [84] that the presence of at least one positive feedback loop is the necessary condition for the emergence of multiple steady

states. The interested reader can find the proof of this conjecture in [79]. It is important to note however that the presence of positive feedback loops can lead to the occurrence of multiple steady states if ultrasensitivity also exists [15, 16]. Simple examples of biochemical interactions that can lead to positive feedback loops are self-activating and double-negative transcriptional regulations. Other examples of positive feedback loop systems that can either naturally occur or synthetically be constructed are given in [12, 38, 52, 65].

Decision-making processes which are vital for the functioning of many biological systems emerge as a result of the existence of bistability [18] in the dynamics of such systems. Bistability as a property of many biological systems underlies basic cellular functions such as cell cycle progression [26, 90, 94], cell fate determination [36] and apoptosis [8, 48]. The importance of bistability has also been addressed in the study of chromatin silencing and epigenetic switches [20, 74]. In the past two decades, several interesting artificial bistable switches have been synthesized [7, 12, 25, 45]. Mathematically speaking, bistability represents the ability of a dynamical system to have two distinct stable steady states for appropriately adjusted parameter values. In situations like cell differentiation or division where certain decisions have to be made by a cell, existence of bistability is crucial since there are no intermediate fates for the cell. Therefore, in the presence of environmental stimuli, because of the existence of a switch-like response, the cell can make a clear-cut decision about its fate. A very famous model system in prokaryotic organisms is the *lac* operon in *Escherichia coli* [72, 80]. The three genes *lacZ*, *lacY* and *lacA* of the system are responsible for the metabolism and absorption of disaccharide lactose. When the lactose is not available in the medium, a repressor protein inhibits the transcription of the genes by binding the operator sites. This puts the switch in the off-state. In the presence of lactose, the switch will be on as the repressor protein unbinds and the transcription of the genes starts. In eukaryotic organisms, a well-known genetic switch is implemented by the galactose metabolic network in *Saccharomyces cerevisiae*. In the absence of glucose, as the main energy source, this model organism metabolizes galactose through Leloir metabolic pathway [13] which is regulated by a set of regulatory proteins and enzymes that define altogether the *GAL* regulon. The *GAL* network has been thoroughly investigated for the emergence of bistability [1, 6, 93].

One standard mathematical way to illustrate the bistability is through the demonstration of hysteresis behavior which is one of the properties of bistable

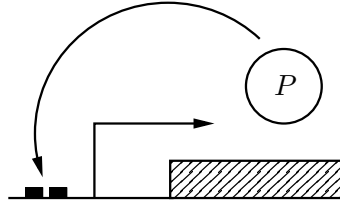


Figure 1.3: A simple positive feedback loop in which a protein enhances the transcription of its own gene.

dynamical systems. For this purpose, we study a one-gene positive feedback loop in which a transcription factor enhances the production of its own gene. Figure (1.3) shows that the protein P binds and activates a promoter to produce itself in a self-activating system. This simple positive feedback loop can easily be represented by the following one-dimensional dynamical system

$$\dot{P} = b + v_{max} \frac{P^n}{K_d^n + P^n} - \gamma P := F(P, \Theta), \quad (1.4)$$

where b is the basal expression rate, v_{max} is the maximum rate of promoter activity, K_d is the equilibrium dissociation constant of P -promoter binding, n is the Hill number and $\Theta \subseteq \mathbb{R}^5$ is the vector of parameters. Equation (1.4) is a simplified version of the complete model with the mRNA dynamics. Here, we assume that the mRNA dynamics are faster than the protein dynamics so that we can apply the quasi-steady state assumption [77] to get equation (1.4). This simple system was first studied by Griffith [30] in 1968 for the existence of bistability. The steady states of system (1.4) are given by putting the right hand side of the system equal to zero

$$\Gamma(P; \Theta) = \{P \mid b + v_{max} \frac{P^n}{K_d^n + P^n} - \gamma P = 0\}. \quad (1.5)$$

Figure (1.4) depicts the graph of steady state equation (1.5) as a function of K_d for selected parameter values. The diagram is a one-parameter bifurcation diagram and the curve is called a hysteresis curve. Later, in this chapter, we present a rigorous mathematical definition of bifurcation and investigate the diagrams of two bifurcations which are specifically related to the emergence of bistability. As shown in Figure (1.4), the threshold for a transition from the lower to the higher branch of steady states is different from a transition in a reverse direction. Because of the existence of this difference, systems with hysteresis behavior are believed to be capable of demonstrating memory. This can be explained in Figure (1.4) as the value of K_d is varied; any transition

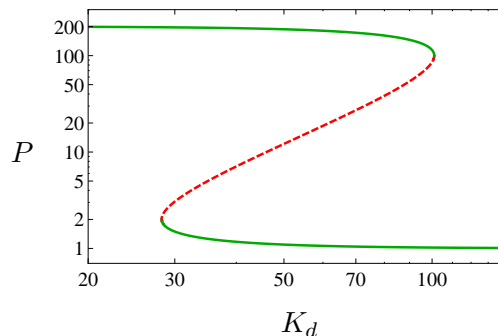


Figure 1.4: Hysteresis curve for system (1.4) for $n = 2$, $v_{max} = 200$, $b = 1$ and $\gamma_P = 1$. Thresholds for low-to-high and high-to-low state transitions are determined by the two knees of the curve. For the values of K_d between the two knees, system (1.4) has one unstable and two stable steady states which are illustrated by the dashed and solid curves.

from the low to the high state by decreasing K_d to values below the low-to-high threshold, will keep the system in the high state even if K_d increases to values between the low-to-high and high-to-low state thresholds. The two thresholds are determined by the two knees of the hysteresis curve which will be later shown to define two saddle-node bifurcation points. It is clear that for values of K_d between the two knees, system (1.4) has three steady states; two stable states in the low and high branches, shown by the solid curves, and one unstable state in the middle branch, depicted by the dashed curve. It is clear from the figure that bistability vanishes at the two saddle-node bifurcation points as a result of a collision between the unstable and stable steady states. This in particular suggests that the unstable steady state is key to the existence and maintenance of bistability. As we will explain later, the unstable steady state plays a major role in the robustness of bistability.

1.5 Robustness

The notion of robustness is long known as a significant and vital characteristic of living systems. A classical example of robust biological systems is the chemotactic signaling pathway in *Escherichia coli* [3, 9] in which variations in the concentration of the nutrient temporarily change the cells' motion mode. This property of the cells is also called adaptability to changing environment. Robustness has also been observed in metabolic networks [78] and circadian rhythm [29].

Robustness means that some specific properties and functions of physical and

living systems are retained under internal and external perturbations [42, 43, 44, 82]. This definition is very broad and needs to be made precise by defining what we exactly mean by the specific properties, in what sense we expect the system to retain these properties and finally how we define perturbations. According to Lodhi et. al [49], specific properties of a system can be either qualitative for which the robustness means to retain the number and type of steady states and oscillatory solutions, or quantitative for which the robustness means to retain for example the frequency and period of an oscillatory solution. They also argue that perturbations can be categorized into three classes: perturbations in the dynamics of the system defined by the vector field F in equation (1.1), the initial conditions, and the parameter values.

Robustness analysis methods are mainly categorized into two main classes, namely, global and local methods [81, 99]. Global methods deal with the entire parameter space of a system and investigate features and characteristics of specific regions of the parameter space for which different dynamical behaviors like oscillations and/or bistability emerge. On the contrary, local methods consider specific parameter values and study changes in the model behavior under perturbations in these parameter values. For the purpose of a global robustness analysis, we can use the bifurcation theory and construct the bifurcation diagrams in the parameter space of a dynamical system. A bifurcation diagram gives the specific information on the domain of a particular dynamical behavior like bistability and/or oscillations. Bifurcation diagrams have been long used for the model evaluation and robustness analysis of biochemical systems [60]. For example, Ma & Iglesias [51] have used the bifurcation diagram to define a measure of robustness for a single parameter in an oscillating system, and Morohashi et al. [58] have investigated the shape and smoothness of bifurcation boundaries and studied the effects of these features of bifurcation diagram on the robustness of oscillations in the *Xenopus* cell cycle oscillator. A very well-known local robustness analysis method is the sensitivity analysis that studies sensitivity of systems' features like the steady states to parametric perturbations. For example, parametric sensitivity analysis has been employed for the sensitivity analysis of stable [17] and unstable [88] steady states to measure their robustness at the presence of parameter perturbations.

1.5.1 Bifurcation theory

Bifurcation theory [31, 46] is a powerful mathematical tool for studying qualitative changes in the family of solutions of a parameter-dependent dynamical

system as parameters are varied. By qualitative changes, we mean changes in the number or stability of steady states of a dynamical system. Bifurcations are depicted in bifurcation diagrams where the qualitative changes are presented in a diagram consisting of state variables and parameters. In the following, we present two well-known bifurcations which are key to the emergence of bistability in dynamical systems.

1.5.1.1 Saddle-node (fold) bifurcation

Saddle-node bifurcation is a local bifurcation in which two steady states move toward each other, collide and disappear when a parameter is varied in a specific direction in the parameter space. The normal form of this bifurcation is given by the following one-dimensional dynamical system [46]

$$\dot{x} = F(x, \alpha) = \alpha + sx^2, \quad (1.6)$$

where $x \in \mathbb{R}$, $\alpha \in \mathbb{R}$ is the bifurcation parameter, and $s = \pm 1$. For $s = 1$, system (1.6) has two steady states, $x = \sqrt{-\alpha}$ and $x = -\sqrt{-\alpha}$ if $\alpha < 0$, and no steady states if $\alpha > 0$. The bifurcation diagram of system (1.6) is shown in Figure (1.5). According to the bifurcation diagram, starting from $\alpha < 0$, if the

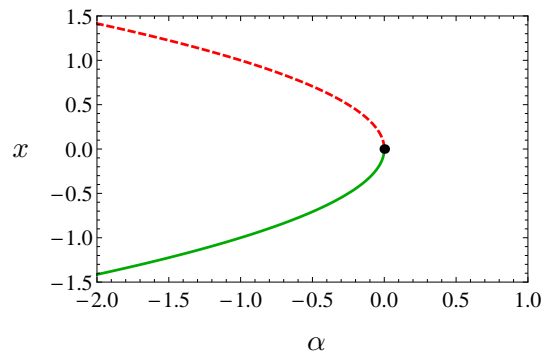


Figure 1.5: The saddle-node bifurcation diagram. On the left half of the plane, system (1.6) has two steady states, the lower stable (solid curve) and the upper unstable (dashed curve) steady states. As α increases, the two branches of steady states move toward each other and collide at the origin and disappear.

value of α is increased, two branches of steady states collide at the origin and disappear for positive values of the bifurcation parameter. In the figure, the solid curve represents the branch of stable steady states while the dashed curve denotes the branch of unstable steady states.

1.5.1.2 Cusp bifurcation

Cusp bifurcation is a local bifurcation whose occurrence divides a two dimensional parameter space of a dynamical system into two topologically different regions; namely, bistability and monostability regions. The normal form of the cusp bifurcation is defined by a one-dimensional dynamical system with two parameters as follows [46]

$$\dot{x} = F(x, \alpha) = \alpha + \beta x + s x^3, \tag{1.7}$$

where $x \in \mathbb{R}$, $\alpha, \beta \in \mathbb{R}$ are the bifurcation parameters, and $s = \pm 1$. For $s = 1$, Figure (1.6) depicts the bifurcation diagram of system (1.7). Figure (1.6:a) illustrates the three-dimensional steady state manifold. The projection of the

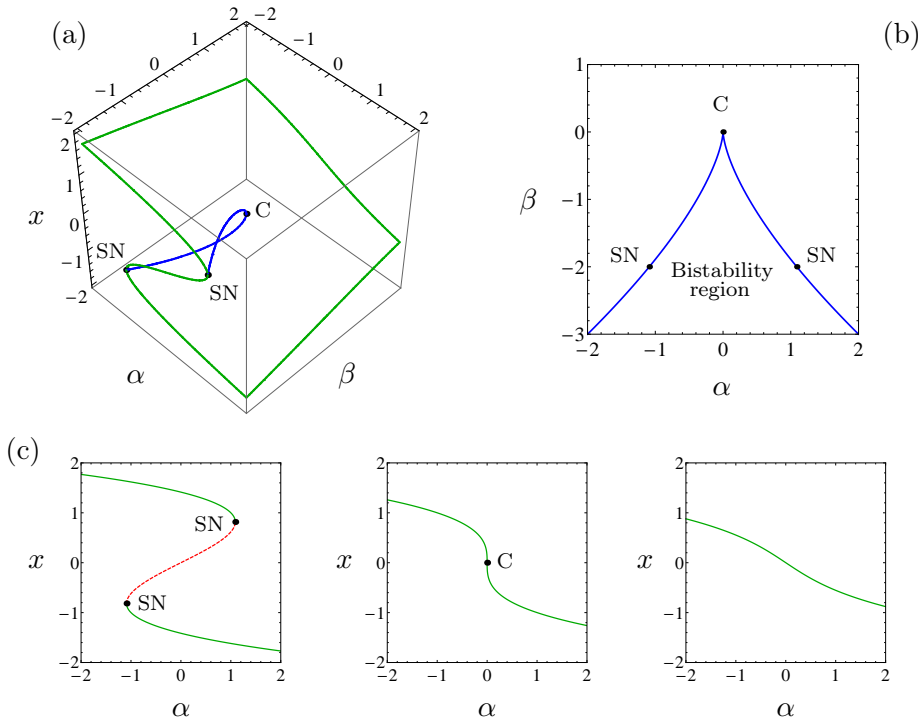


Figure 1.6: The cusp bifurcation diagram. (a) The three dimensional steady state manifold with the curves of saddle-node bifurcation labeled with SN. (b) The projection of steady state manifold into the parameter space. Inside the bistability region, system (1.7) has two distinct stable steady states. (c) One dimensional steady state manifold for $\beta = -2$ (left), $\beta = 0$ (middle), $\beta = 1.5$ (right). In the interval between the two knees, system (1.7) has three steady states, the upper and lower stable and the middle unstable steady states.

steady state manifold into the two-dimensional parameter space is shown in Figure (1.6:b). Inside the bistability region, the system has two distinct stable

steady states. This can also be seen in Figure (1.6:c) where for an interval of α values between the two saddle-node bifurcation points (SN), system (1.7) has three steady states, the lower and upper stable and the middle unstable steady states.

Construction of bifurcation diagrams can be a first step to acquire information on the robustness of dynamical characteristics like bistability as the bifurcation boundaries tell us where the system loses its structural stability as a result of parameter perturbations. As we mentioned earlier, bifurcation diagrams provide a global information on the robustness of dynamical features in the parameter space. In the following, we will explain a local method with which the sensitivity of a dynamical system's properties like steady states to individual parameters can be measured.

1.5.2 Parametric sensitivity analysis

The uncertainty over the parameter values can happen because of the dependence of the system on unknown external factors [37]. Sensitivity analysis is a classical technique that can be used as a measure of parametric robustness [89]. The sensitivity analysis [95] studies the sensitivity of a system to parameters in a vicinity of nominal values in the parameter space. The parametric sensitivity S_c of a physical quantity c to a parameter k is defined with the following simple derivative

$$S_c(k) = \frac{dc}{dk}. \quad (1.8)$$

With an appropriate rescaling, equation (1.8) becomes

$$S_c(k) = \frac{k}{c} \frac{dc}{dk}. \quad (1.9)$$

Equation (1.8) has physical dimensions and is called the absolute sensitivity, while equation (1.9) is dimensionless and is called the relative sensitivity as it defines the relative rate of change of c with respect to the parameter k . Equation (1.9) can also be called the logarithmic sensitivity since it can be taken as the logarithmic derivative of the variable c with respect to k .

1.6 The open-loop approach: The concept of loop opening in biological feedback systems

One important question in the analysis of bistability in large complex biochemical networks is whether it is possible to predict the presence of bistability with-

out going through complicated mathematical calculations. Angeli et al. [5] have recently formulated a method to prove the existence of bistability in large feedback loop systems based on the open-loop approach. They have shown that if the feedback loop is opened, the open-loop response of the network is sufficient to guarantee bistability if it is a sigmoidal monostable steady-state response to constant inputs and has three intersections with the identity line, and in addition, there are no negative feedback loops. The latter assumption makes the system strongly monotone [4]. The method proposed by Angeli and his colleagues reduces the complexity of analyzing large systems with many variables and parameters to studying a single algebraic equation which gives the output response as a function of a constant input. We illustrate the open-loop approach by opening the positive feedback loop in system (1.4). We discuss in particular two main properties of the open-loop system, namely, the input-output steady state response function which expresses the output of the open-loop system as a function of a constant input, and the sensitivity of the output function to the input defined by equation (1.9). We study both the closed-loop and open-loop versions of system (1.4) and establish relations between the bifurcation diagram and the open-loop system features with regard to bistability.

1.6.1 The self-activating system

1.6.1.1 The closed-loop system

Bistability is about having three steady states, two of which are stable and the other is unstable. The number of steady states of a dynamical system like system (1.4) can be obtained by putting the right hand side of the equation equal to zero. This equation is a polynomial of degree $n + 1$ and therefore, it is clear that for bistability we must have $n > 1$. In the simplest case for $n = 2$, the steady state equation becomes a polynomial of degree three which gives at most three real solutions depending on the parameter values. The distribution of steady states in the parameter space is determined by the roots of the discriminant of the steady state equation. These roots define the boundaries of bistability region illustrated in Figure (1.7) for selected parameter values. The boundaries represent two curves of saddle-node bifurcation and their intersection gives birth to a cusp bifurcation point in the (b, K_d) -space. According to bifurcation diagram (1.7), for lower values of basal expression b , the bistability range expands in the direction of K_d . This range shrinks as the value of b increases.

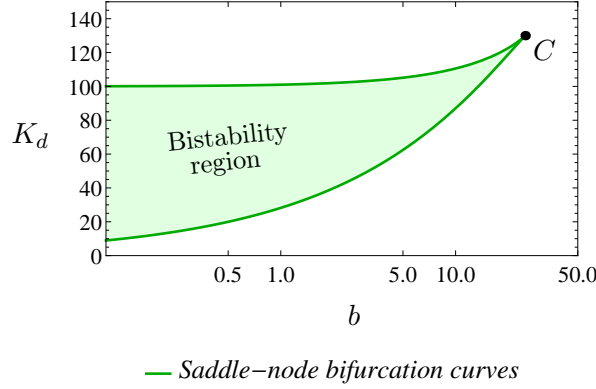


Figure 1.7: Bifurcation diagram of system (1.4) for $v_{max} = 200$, $n = 2$ and $\gamma = 1$. The two boundaries of the bistability region are saddle-node bifurcation curves and their intersection point C is a cusp bifurcation point.

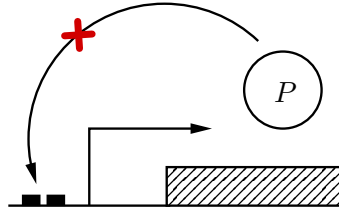


Figure 1.8: The open-loop version of system (1.4). The positive feedback loop is opened where the protein binds the promoter.

1.6.1.2 The open-loop system

Figure (1.8) shows that the positive feedback loop can be opened at the point where the protein binds the promoter. The open-loop equation is achieved by replacing P in the Hill function with a constant variable ω which defines the input to the system. The other P in the degradation term plays the role of the output and is renamed as η . Therefore, equation (1.4) becomes

$$\dot{\eta} = b + v_{max} \frac{\omega^n}{K_d^n + \omega^n} - \gamma\eta. \quad (1.10)$$

The loop opening in system (1.4) can be experimentally done by replacing the native promoter with an exogenously inducible one. As a result, the promoter will not be under the control of the protein P anymore. The closed-loop system (1.4) is reconstructed by putting $\eta = \omega$. The steady state open-loop response of system (1.10) is achieved by putting the right hand side of equa-

tion (1.10) equal to zero which results in

$$\eta = \frac{1}{\gamma} \left(b + v_{max} \frac{\omega^n}{K_d^n + \omega^n} \right) := R_\eta(\omega, \Theta), \quad (1.11)$$

where $\Theta \subseteq \mathbb{R}^5$ is the vector of parameters. The graph of response function (1.11) is depicted in Figure (1.9) for selected parameter values. Steady states of the

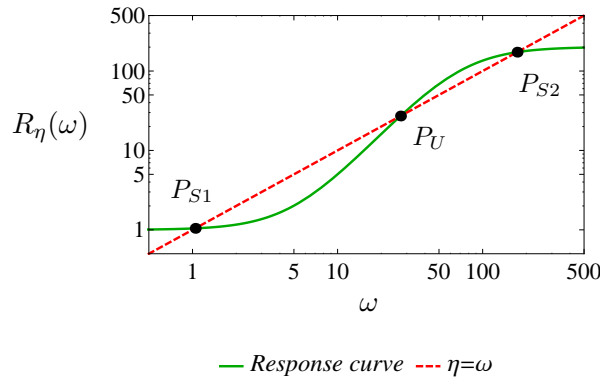


Figure 1.9: The response curve of system (1.10) for $v_{max} = 200$, $n = 2$, $\gamma = 1$, $b = 1$ and $K_d = 70$. Intersection of the steady state open-loop response (1.11) with the identity line where $\eta = \omega$, yields the steady states of the closed-loop system (1.4). The stable points are denoted by P_{S1} and P_{S2} , and the unstable point is labeled with P_U .

closed-loop system (1.4) are given by the intersections of the response curve with the identity line on which $\eta = \omega$. The middle unstable steady state is labeled with P_U and the lower and upper stable steady states are denoted by P_{S_i} , $i = 1, 2$. As we mentioned earlier in this chapter, another quantity related to the open-loop system which will be employed in the robustness analysis, is the sensitivity of the output response to the input. This sensitivity gives us valuable information on the ultrasensitivity of the response curve since it can be used to measure the curve steepness. Using equation (1.9), the logarithmic sensitivity of the output (η) to the input (ω) is defined as follows

$$S_\eta^\omega(\omega, \Theta) = \frac{\omega}{R_\eta(\omega, \Theta)} \frac{d}{d\omega} R_\eta(\omega, \Theta). \quad (1.12)$$

It has been discussed in [18] that for the existence of multiple steady states, the function (1.12) must be greater than one at the unstable steady state. Figure (1.10) shows the relationship between the response and sensitivity diagrams for fixed parameter values inside the bistability region (1.7). In the response diagram (1.10:a), the two lines that connect the origin (the origin is not shown

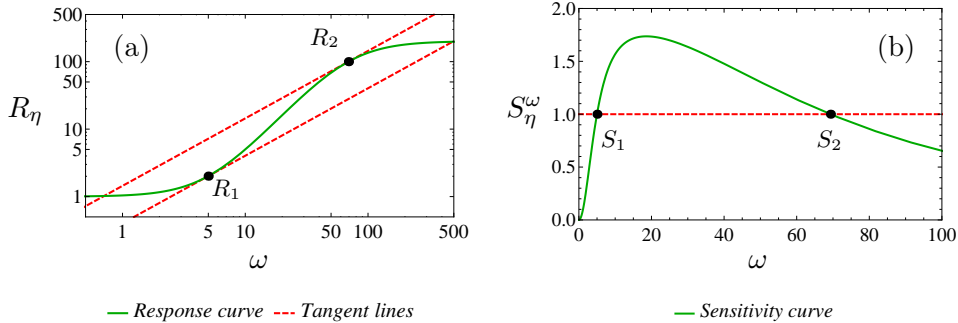


Figure 1.10: Response (a) and sensitivity (b) diagrams of system (1.10) for $v_{max} = 200$, $n = 2$, $\gamma = 1$, $b = 1$ and $Kd = 70$. The two tangent lines to the response curve determine the interval in which the sensitivity is greater than one. The points R_1 and R_2 in the response diagram correspond to the two points S_1 and S_2 in the sensitivity diagram.

because the response curve is plotted in the logarithmic scale) to $R_1 : (\omega_1, \eta_1)$ and $R_2 : (\omega_2, \eta_2)$ are tangent to the curve. According to equation (1.12), this means that $S_\eta^\omega(\omega_i) = 1$, $i = 1, 2$ as the ratio becomes one at these points. This is also illustrated in Figure (1.10:b); the intersection of the sensitivity curve with the dashed horizontal line gives birth to the two points $S_1 : (\omega_1, 1)$ and $S_2 : (\omega_2, 1)$ which exactly correspond to R_1 and R_2 . Furthermore, for every $\omega^* \in (\omega_1, \omega_2)$, $S_\eta^\omega(\omega^*) > 1$, while for $\omega^* \in \mathbb{R} - [\omega_1, \omega_2]$, $S_\eta^\omega(\omega^*) < 1$. A comparison between Figures (1.9) and (1.10:a) suggests that in a bistable regime, the identity line must lie between the two tangent lines. This shows that the sensitivity of the open-loop response function to the input at the unstable steady state is greater than one which means that the response curve is ultrasensitive at this point. In the next chapter, we will employ the open-loop approach to study bistability robustness in some prototypical feedback systems and to reconstruct the bistable behavior of the *GAL* network in *Saccharomyces cerevisiae*.

Chapter 2

Results

In this chapter, we study bistability and its robustness in prototypical positive feedback loop systems by using the open-loop approach. In the first section, we address the issue of bistability robustness by exploring the extrema of bifurcation boundaries in the parameter space. The emergence of such extrema enlarges the bistability range of a single parameter and therefore contribute to the robustness of bistability. We in particular show that a negative feedback loop can create the possibility of extending the bistability range of a parameter. In the second section, we peruse a different approach to the study of bistability robustness by studying the unstable steady state sensitivity to parameters. As we discussed before, the preservation of unstable steady state of a bistable system against parameter perturbations is key to the maintenance of bistability. Our goal is specifically to detect parametric regions inside the bistability area in which the sensitivity of the unstable steady state to parameters can be minimized so that the parameter perturbations have the least effect on the unstable steady state. We continue our investigation of system (1.4) and establish our main results on the bistability robustness by using the open-loop sensitivity. We later apply our results to two examples of higher dimensional systems that have homodimerization and titration as the ultrasensitive mechanisms. Finally, in the third section, we study the galactose network in *Saccharomyces cerevisiae* and develop a mathematical model to reconstruct the bistable behavior of the network. We show how the experimental data extracted from different layers of the network can be used to estimate the value of main parameters of the model by performing the nonlinear regression. We also discuss the computational challenges that we face in using the nonlinear regression for building the mathematical model for the galactose network. Our mathematical model proves the significance of homodimerization and titration mechanisms in creating bistability in the galactose network.

2.1 Exploring the extrema of the bistability range of a single parameter

As we discussed in Chapter 1, bifurcation diagrams provide the very first valuable information on the robustness of a dynamical characteristic like bistability by giving the exact boundaries of the parametric region in which the desired characteristic behavior emerges. In the case of system (1.4), bifurcation diagram (1.7) depicts the boundaries of bistability region for two parameters b and K_d . Moreover, as illustrated in the figure, the cusp bifurcation point C also defines an extremum for the bistability range of these two parameters. In other words, the cusp point determines the b and K_d extremal bistability values beyond which the emergence of bistable behavior is not possible. One important question is whether it is possible to extend the bistability range of parameters by moving the cusp point. For example, in Figure (1.7), if the cusp point is moved to the right or elevated, the bistability range of the parameters b and K_d can be extended. This is a very important observation for the robustness of bistability with regard to a single parameter variations since any extension in the parametric range means that the bistable behavior of the system is less likely to disappear as a result of parameter perturbations. In this section, we are going to explore such possibility in positive feedback loops. We are in particular interested to see whether a negative feedback loop when interacting with a positive feedback loop, can create the possibility of an extension in the bistability range of a parameter. Negative regulatory mechanisms such as negative feedback loops are also ubiquitous in many biological systems. They are well-known mainly for their role in creating sustained oscillations [21] and repressing noise [11]. Negative feedback loops can also act as a linearizer and transform a sigmoidal response curve to a linear one [10, 61]. This suggests that negative feedback loops can weaken and eventually eliminate the ultrasensitivity of the response curve which is a necessary condition for having multiple steady states. On the other hand, depending on the architecture of the system, negative feedback loops can increase the nonlinearity of the system and therefore contribute to the ultrasensitivity in the dynamics of the system. There are examples in which coupling between positive and negative feedback loops can extend the range of bistability in a specific architecture [87]. The dual role of negative feedback loops leads us to explore a simple system consisting of a positive and a negative feedback loop. This system is illustrated in Figure (2.1). The system has two main regulatory proteins; there is an activator P and an inhibitor Q . The activator promotes the production of its own gene and the

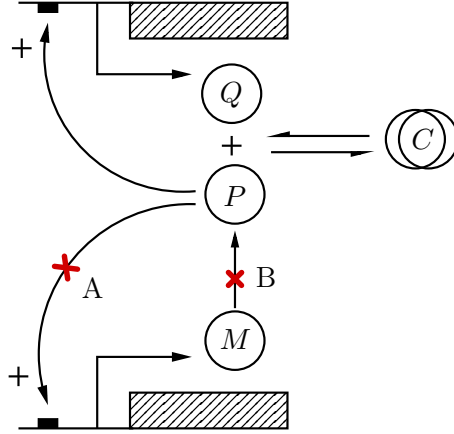


Figure 2.1: A gene regulatory system with a positive and a negative feedback loop. The activator P promotes its own production in a self-activating loop, and induces the production of the inhibitor Q that in turn sequesters P into an inactive complex. The positive feedback loop can be opened at either A (the protein level) or B (the mRNA level).

inhibitor, and the inhibitor sequesters the activator into an inactive complex C that cannot bind the promoters. The self-activation of P constitutes a positive feedback loop, and the positive regulation of Q by P together with the negative regulation of P by Q closes a negative feedback loop. Molecular titration or sequestration is a very strong source of nonlinearity in biochemical systems and is ubiquitous in many regulatory networks like the *GAL* network. We will give a very short introduction to the titration mechanism in the next section where we study a positive feedback loop with molecular titration. The system shown in Figure (2.1) is modeled by the following set of differential equations

$$\begin{aligned}
 \dot{M} &= b_M + v_P \frac{P}{K_{dP} + P} - \gamma_M M, \\
 \dot{P} &= \mu M - k_{on} P Q + k_{off} C - \gamma_P P, \\
 \dot{Q} &= b_Q + v_Q \frac{P}{K_{dQ} + P} - k_{on} P Q + k_{off} C - \gamma_Q Q, \\
 \dot{C} &= k_{on} P Q - k_{off} C - \gamma_C C,
 \end{aligned} \tag{2.1}$$

where b_M and b_Q are the basal expression rates for the activator mRNA M and the inhibitor Q respectively, v_P and v_Q are the maximum production rates of the promoters, μ is the translation rate of the mRNA into protein, and γ_M , γ_P , γ_Q and γ_C are the degradation rate constants of components. The parameters

k_{on} and k_{off} are association and dissociation rate constants of protein-protein binding and K_{dP} and K_{dQ} are the equilibrium dissociation constants of protein-promoter binding.

In the first step, we put $b_M = 0$ and study both the closed-loop and open-loop systems. This assumption dramatically reduces the complexity of algebraic equations. The steady state equation of the closed-loop system (2.1) is given by the following algebraic equation

$$P \left(-\gamma_P P^2 + \left(\frac{\mu}{\gamma_M} \frac{v_P P}{K_{dP} + P} - \frac{v_Q P}{K_{dQ} + P} - b_Q - \kappa \right) P + \frac{\mu \kappa}{\gamma_M \gamma_P} \frac{v_P P}{K_{dP} + P} \right) = 0, \quad (2.2)$$

where κ is a lumped parameter and is defined by the following equation

$$\kappa = \frac{\gamma_P \gamma_Q}{\gamma_C} \left(\frac{k_{off} + \gamma_C}{k_{on}} \right). \quad (2.3)$$

For simplicity, we assume that the equilibrium dissociation constant of P to both promoters are equal with each other, that is, $K_{dP} = K_{dQ} = K_d$. The distribution of steady states in the parameter space is determined by the roots of the discriminant of the steady state equation (2.2). The bistability region in the case of system (2.1) is enclosed by a saddle-node and a transcritical bifurcation curve. Transcritical bifurcation is related to the stability exchange between two steady states rather than the creation and elimination of them [46]. The intersection of saddle-node and transcritical bifurcation curves defines a saddle-node-transcritical bifurcation point [73]. Figure (2.2) shows the bifurcation diagram of system (2.1) in two different parameter spaces, i.e., the (κ, b_Q) - and (κ, K_d) -space. Both diagrams in Figure (2.2) show that the locus of saddle-node-transcritical bifurcation points (SNT points) has a maximum in the direction of b_Q and K_d , meaning that the bistability range of the parameter κ can be maximized to the extremum of the locus. The coordinates of the maximum point are given by

$$\begin{aligned} b_Q &= \frac{1}{4} \frac{\mu^2 v_P^2 - \gamma_M^2 v_Q^2}{\mu v_P \gamma_M}, \\ K_d &= \frac{1}{2} \frac{\mu v_P - \gamma_M v_Q}{\gamma_P \gamma_M}, \\ \kappa &= \frac{1}{4} \frac{(\mu v_P - \gamma_M v_Q)^2}{\mu v_P \gamma_M}. \end{aligned} \quad (2.4)$$

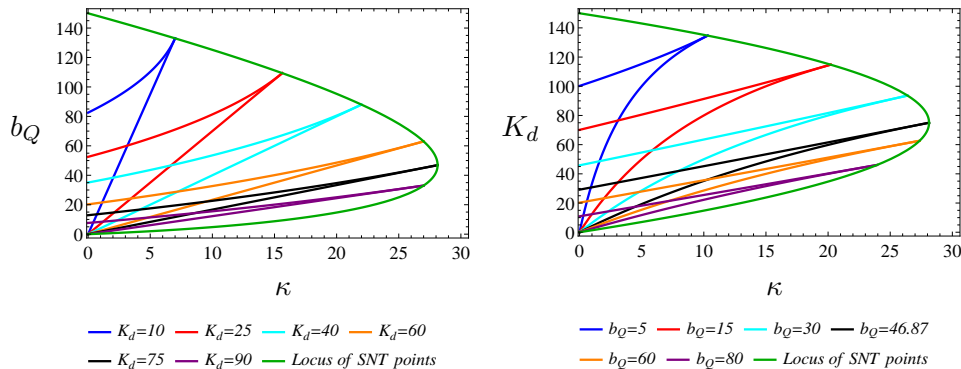


Figure 2.2: Bifurcation diagram of system (2.1) in two different parameter spaces for $v_P = 200$, $v_Q = 50$, $\gamma_P = \gamma_M = 1$ and $\mu = 1$. The locus of saddle-node-transcritical (SNT) bifurcation points has a maximum in the direction of both b_Q and K_d . This means that the bistability range of κ can be maximized.

The bifurcation diagrams in Figure (2.2) can very well explain how a negative feedback loop can increase the bistability range of a parameter like κ . It is interesting to see that the contribution of the negative feedback loop to the bistability has a defining point which is given by the maximum of the locus of the saddle-node-transcritical bifurcation points. It is important to note that since the Hill number in the positive feedback loop is equal to one, the ultrasensitivity necessary for the emergence of bistability, is solely provided by the titration mechanism in the negative feedback loop. The ultrasensitivity contributes to the bistability range of κ until the value of this parameter reaches the maximum of the saddle-node-transcritical locus. After reaching this point, further increase in the value of K_d or b_Q leads to the shrinkage of the range, meaning that the negative feedback starts to weaken bistability in the direction of the parameter κ .

Now that we have detected the maximum of the bistability range for a parameter like κ , we are interested to investigate whether we can formulate mathematical conditions with which it is possible to detect such maximum points in an arbitrary parameter space. In particular, we are interested to see if the open-loop approach can help us achieve this goal. For this purpose, we open the positive feedback loop in system (2.1). The loop can in fact be opened in two different ways as shown in Figure (2.1). One opening can be done at the protein level where P binds the promoter, and the other can be done at the mRNA level where the mRNA is translated into protein. For the opening from the protein level, the open-loop version of system (2.1) is given by replacing P in the first

equation by a constant ω

$$\dot{M} = b_M + v_P \frac{\omega}{K_{dP} + \omega} - \gamma_M M, \quad (2.5)$$

and the rest of equations remain the same. In this open-loop version, P is the output of the system and therefore, we call this system as the P -system. For the opening from the mRNA level, M is replaced by ω in the second equation of system (2.1) as

$$\dot{P} = \mu \omega - k_{on} P Q + k_{off} C - \gamma_P P, \quad (2.6)$$

and the rest of equations remain the same. In this open-loop version, M serves as the output of the system and the system itself is referred to as the M -system. It is straightforward to calculate the open-loop response and sensitivity of both P - and M - systems. For the P -system, the steady state input-output equation reads as follows

$$-\gamma_P P^2 + \left(\frac{\mu}{\gamma_M} \frac{v_P \omega}{K_d + \omega} - \frac{v_Q P}{K_d + P} - b_Q - \kappa \right) P + \frac{\mu \kappa}{\gamma_M \gamma_P} \frac{v_P \omega}{K_d + \omega} = 0, \quad (2.7)$$

and for the M -system, the response function is achieved by solving

$$-\gamma_P P^2 + \left(\mu \omega - \frac{v_Q P}{K_d + P} - b_Q - \kappa \right) P + \frac{\kappa}{\gamma_P} \mu \omega = 0, \quad (2.8)$$

$$P = \frac{\gamma_M K_d M}{v_P - \gamma_M M}.$$

The corresponding sensitivity functions, S_P^ω and S_M^ω for P and M systems can be calculated using equation (1.12). For the P -system, it is interesting to observe that the variations in the value of b_Q make the maximum of sensitivity curves change in a nonmonotone fashion. Figure (2.3) illustrates the sensitivity curves of the P -system for different values of b_Q and K_d . As shown in the figure, only the variations of b_Q create a nonmonotone change in the maximum of sensitivity curves. This is a first impression as to whether the open-loop sensitivity can help detect the maximum of the locus of saddle-node-transcritical points in the bifurcation diagram. In particular, we can plot a curve in the (κ, b_Q) -space on which the maximum of sensitivity curves reaches its maximum value. This curve is calculated by solving the two following equations

$$\frac{d}{d\omega} S_P^\omega(\omega, \Theta) = 0 \quad \text{and} \quad \frac{d}{d\theta} S_P^\omega(\omega, \Theta) = 0, \quad (2.9)$$

for $\theta = b_Q$ with Θ as the vector of all parameters. The resulting curve that expresses b_Q as a function of κ is shown in Figure (2.4). We refer to this

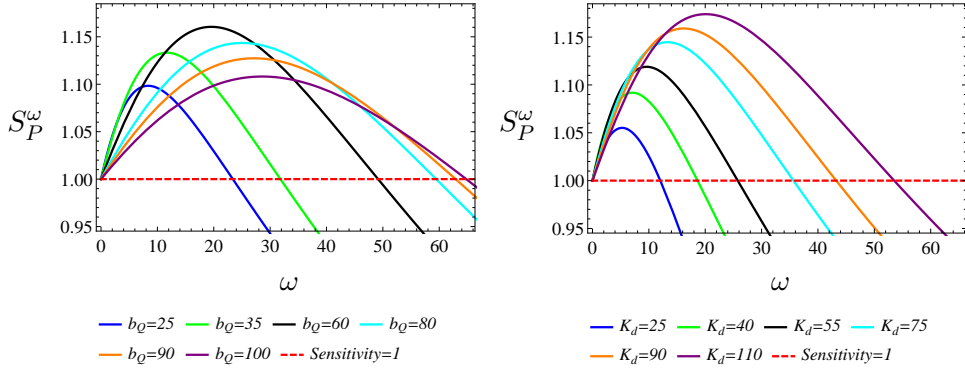


Figure 2.3: Sensitivity diagram of the P -system for $v_P = 200$, $v_Q = 50$, $\gamma_P = \gamma_M = 1$ and $\mu = 1$, and for $K_d = 75$ in the left diagram and $b_Q = 40$ in the right diagram. Variations of b_Q create a nonmonotone change in the maximum of sensitivity curves. This is not the case for the parameter K_d .

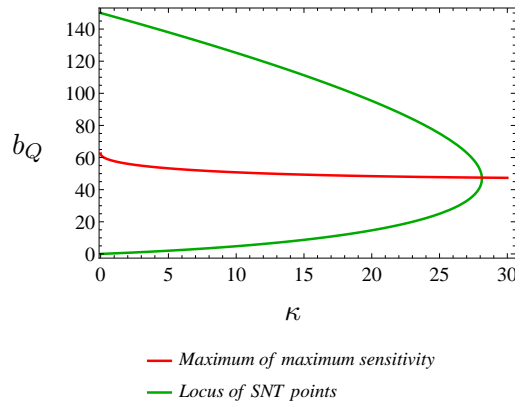


Figure 2.4: The locus of saddle-node-transcritical bifurcation points and its intersection with the locus of maximum of maximum sensitivity for $v_P = 200$, $v_Q = 50$, $\gamma_P = \gamma_M = 1$ and $\mu = 1$. The two curves intersect at the maximum of saddle-node-transcritical locus which gives the biggest bistability range for κ .

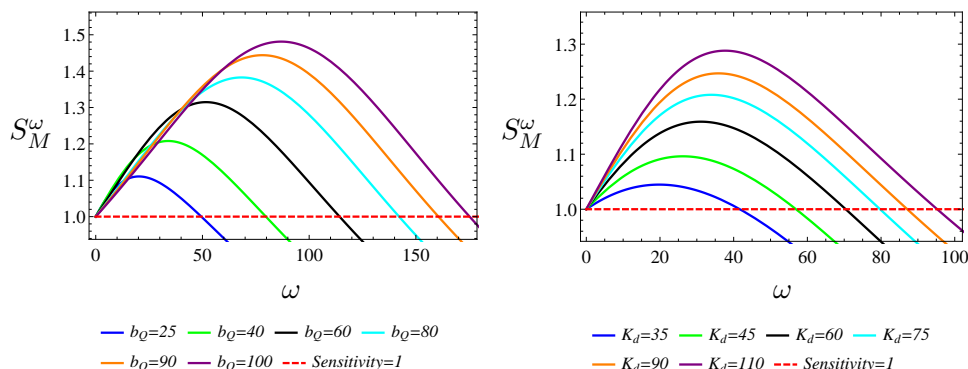


Figure 2.5: Sensitivity diagram of the M -system for $v_P = 200$, $v_Q = 50$, $\gamma_P = \gamma_M = 1$ and $\mu = 1$ and for $K_d = 75$ in the left diagram and $b_Q = 40$ in the right diagram. The maximum of sensitivity curves varies monotonically with both b_Q and K_d .

curve as the maximum of maximum sensitivity curve. It is very interesting to observe that the curve of maximum of maximum sensitivity intersects the locus of saddle-node-transcritical points at the rightmost point which gives the biggest bistability range for the parameter κ . This means that the open-loop sensitivity of the P -system can successfully predict the maximum of the saddle-node-transcritical curve for b_Q . We can also check the M -system in a similar fashion. The sensitivity diagram for the M -system is shown in Figure (2.5). Interestingly, in the case of M -system, variations in the value of both b_Q and K_d fail to create a nonmonotone change in the maximum of sensitivity. This already suggests that the M -system may not be able to yield any results for the detection of the maximum of the locus of saddle-node-transcritical points in the (κ, K_d) -space.

In the next step, we study system (2.1) with $b_M \neq 0$. We carry out the same analysis for the corresponding P and M systems. Since adding this new parameter makes the calculations quite difficult and tedious, we drop the Hill function production of the inhibitor Q by P and only keep the positive feedback loop which is necessary for bistability. The resulting system still shows the essential characteristics of the original system with the negative feedback loop. In particular, the bifurcation and sensitivity diagrams, as we will shortly discuss, have the same features as we studied above. For the P -system with basal for the activator, the sensitivity diagrams for both varying b_Q and K_d show the same pattern as in Figure (2.3). Figure (2.6) shows that b_Q variations create a nonmonotone change in the level of maximum sensitivity and K_d variations still

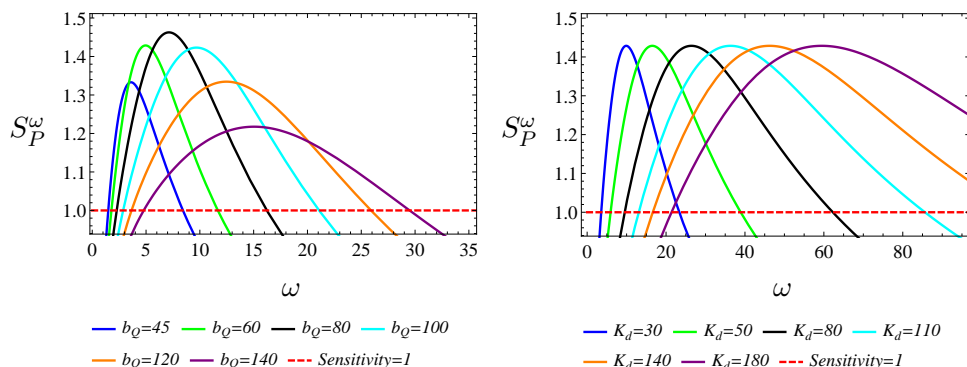


Figure 2.6: Sensitivity diagram of the P -system with basal for the activator ($b_M \neq 0$) for $v_P = 200$, $b_M = 10$, $\gamma_P = \gamma_M = 1$ and $\kappa = 5$, and for $K_d = 15$ in the left diagram and $b_Q = 60$ in the right diagram. Variations of b_Q create a nonmonotone change in the maximum of sensitivity curves. The parameter K_d can only shift the maximum of sensitivity curves to the right or left.

fail to do so. For the M -system with basal for the activator, there is a possibility to demonstrate the nonmonotone change in the maximum of sensitivity curves. It is interesting to see that this phenomenon happens as a result of variations in the value of K_d . The results are shown for the M -system in Figure (2.7). The new results for the M -system with basal for the activator further approves the need for a thorough investigation on how different parameter configurations can lead to the detection of the nonmonotone variations in the maximum of sensitivity. It is also interesting to see if the locus of maximum of maximum sensitivity can predict the maximum point in the locus of bifurcation points in the bifurcation diagram. It is important to note that for a nonzero basal value for the activator ($b_M \neq 0$), the locus of bifurcation points represents a curve of cusp bifurcation points. Figure (2.8) illustrates the intersection of the locus of maximum of maximum sensitivity, calculated by using equation (2.9) for $\theta = b_Q, K_d$, with the locus of cusp bifurcation points in the parameter space. For the P -system, the intersection happens at the maximum of the cusp locus, while for the M -system, the intersection is detected elsewhere. This means that the P -system is still the only open-loop version of the original system that can predict the biggest bistability range for a single parameter like κ and although the maximum sensitivity of the M -system undergoes a nonmonotone variation with K_d , it fails to determine the maximum of the cusp locus.

With all mentioned above, we can conclude that the problem of detecting the maximum point in the locus of bifurcation points (saddle-node-transcritical/cusp)

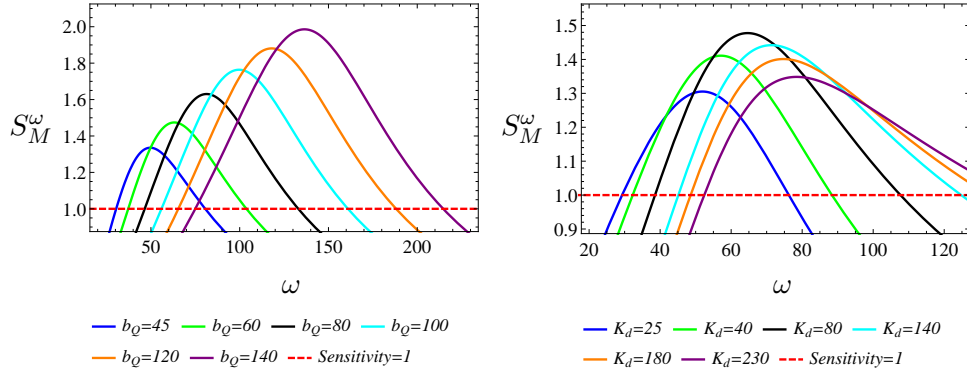


Figure 2.7: Sensitivity diagram of the M -system with basal for the activator ($b_M \neq 0$) for $v_P = 200$, $b_M = 10$, $\gamma_P = \gamma_M = 1$ and $\kappa = 5$, and for $K_d = 70$ in the left diagram and $b_Q = 60$ in the right diagram. The parameter K_d can create a nonmonotone change in the maximum of sensitivity.

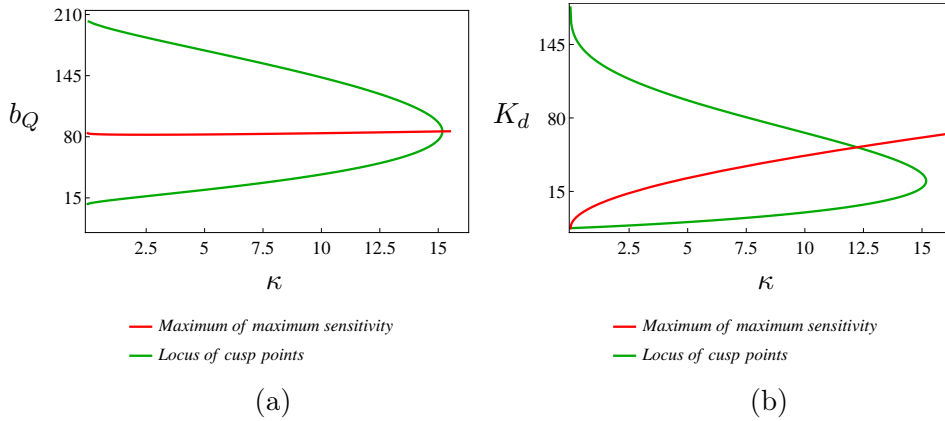


Figure 2.8: The locus of cusp bifurcation points and its intersection with the locus of maximum of maximum sensitivity for $v_P = 200$, $b_M = 10$, $\gamma_P = \gamma_M = 1$ and $\mu = 1$. (a) For the P -system, the two loci intersect at the maximum of the cusp locus. (b) For the M -system, the intersection happens at a point other than the maximum of the cusp locus.

is twofold. Firstly, our studies show that the way of opening the feedback loop can play an important role in determining the parameter configurations that can detect the maximum of the bifurcation points locus. Our investigations also reveal that some parameters can have an essential impact on the desired parameter configurations. This is approved by examining the role of b_M whose presence is necessary for the M -system sensitivity to demonstrate a nonmonotone change in its maximum level. Secondly, at the presence of a nonmonotone change in the maximum sensitivity level, as we saw above, the intersection of the maximum of maximum sensitivity curve with the locus of bifurcation points does not necessarily happen at the maximum of the bifurcation points locus. In this case, the open-loop formulation fails to predict the existence of this point in the bifurcation diagram. For the case of the M -system, the question still remains as to whether it is possible to move the intersection point to the maximum of the cusp locus by varying other parameters. In other words, it may be necessary to include more parameters in our investigations. This question has been recently addressed by Majer et al. [53] where it is shown that the bistability range of a parameter can be maximized if the sensitivity of the open-loop system is maximized with respect to two other parameters. The formulas are general and provide a recipe for choosing the relevant parameters regardless of the way the original system is opened. Therefore, the need to include more parameters in the analysis of the extrema of the bistability range of a single parameter has been shown. In the case of M -system, for example, the extremum of bistability range for b_Q is given if the open-loop system sensitivity is maximized with respect to both K_d and v_P , and the extremum for v_P is achieved if the sensitivity is maximized with respect to K_d and b_Q . The formulation has been used to predict the extrema of the bistability range for different parameters in a single positive feedback system with titration and two positive feedback loop systems with double-positive and double-negative interactions.

2.2 Exploring robust regions of the bistability area

In this section, we pursue a different approach in the analysis of bistability robustness by focusing on the unstable steady state. The unstable steady state of a dynamical system plays a key role in the organization of bistability and its variations under the parameter perturbations are significant to the maintenance of this dynamical characteristic. We explore robust bistability regions by minimizing the sensitivity of the unstable steady state sensitivity to parameters of a system. We use system (1.4) to establish our main results and formulations, and

later, apply our results to two example systems of higher dimensions. One of our main goals in this section is to employ the open-loop sensitivity to formulate mathematical conditions for the detection of the robust bistability regions.

In chapter 1, we discussed that the ultrasensitivity of the response curve at the unstable steady state is the necessary condition for the presence of bistability and its strength can consequently have positive effects on the bistability phenomenon. Therefore, we can expect to have a highly robust bistability when the ultrasensitivity is present at its maximum level. We turn our focus on the response diagram of the open-loop system (1.10) and specifically the locus of unstable steady states on the response curve. Figure (2.9) depicts the response curve (1.11) for different values of K_d inside the bistability region. It is clear

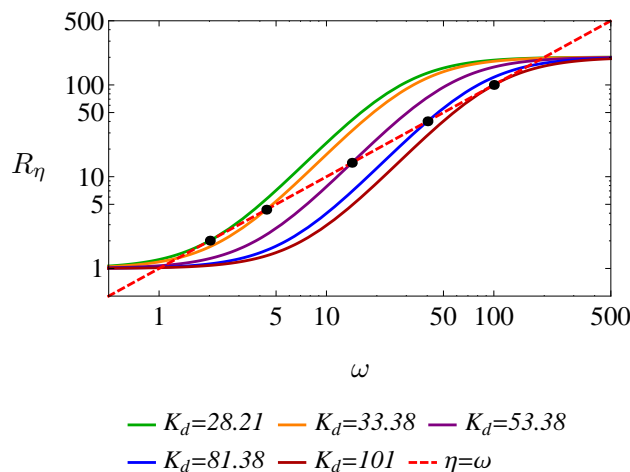


Figure 2.9: The graph of response curve for $v_{max} = 200$, $n = 2$, $\gamma = 1$, $b = 1$ and different values of K_d . The black dots on the intersection of the identity line and the curves represent different positions of unstable steady state of the closed-loop system (1.4).

from the figure that the steepness of the curve at the middle unstable point varies with K_d . A look at the corresponding sensitivity diagram in Figure (2.10) (equation (1.12)) tells us which response curve has the highest steepness at the unstable point. In fact, Figure (2.10) suggests that it is possible to push the unstable steady state to the maximum of sensitivity by varying the value of K_d . The figure shows that for a specific value of this parameter, the response curve can reach the highest possible ultrasensitivity at the unstable steady state. It should be noted that the unstable steady state does not necessarily need to be the maximum of the sensitivity curve. Our goal is in fact to have the maximum

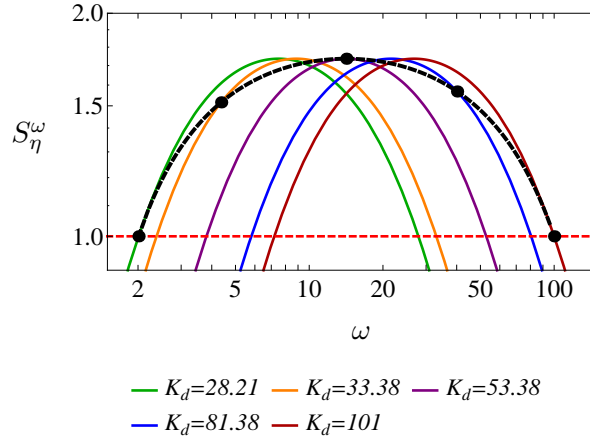


Figure 2.10: The graph of sensitivity curve for $v_{max} = 200$, $n = 2$, $\gamma = 1$, $b = 1$ and different values of K_d . The locus of unstable steady states are denoted by the black dashed curve. The open-loop sensitivity at the unstable steady state reaches its maximum value at $K_d = 53.38$.

sensitivity of the response at the unstable steady state which here happens to be the maximum of a specific sensitivity curve as well. It is straightforward to see why this is the case for K_d in system (1.10). In fact, a look at the response diagram (2.9) suggests that variations of K_d do not have any influence on the upper and lower limits of the response curve. By limits, we mean the basal level in the lower part of the curve as the ω tends to zero and the saturation level in the upper part of the curve as ω tends to infinity. This means that the dynamic range of the response curve, defined as the ratio of the upper and lower limits, does not change with K_d . The invariance of the dynamic range with respect to K_d can also be observed in the sensitivity diagram (2.10) where changes in K_d do not change the highest level of sensitivity which is defined by the maximum point of sensitivity curves. In fact, variations in the value of K_d only shift the sensitivity curves to the right or left.

In a similar fashion, we can construct sensitivity diagrams for other parameters of the system. For v_{max} and b , just like K_d , it is possible to maximize the open-loop sensitivity at the unstable steady state. Figure (2.11) depicts the open-loop sensitivity curves for these two parameters together with the locus of unstable steady states for different values of v_{max} and b . As illustrated in the figure, variations in the value of v_{max} and b define a maximum in the locus of unstable points and this maximum does not coincide with the maximum of the sensitivity curve. Figures (2.10) and (2.11) suggest that the maximization

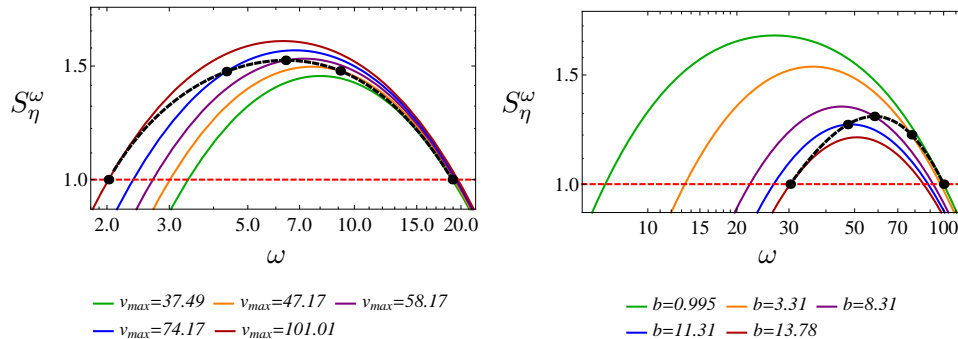


Figure 2.11: The graph of sensitivity curve for $n = 2$, $\gamma = 1$, and for $b = 1$, $K_d = 20$ in (a), and $v_{max} = 200$, $K_d = 101$ in (b). The locus of unstable steady states is denoted by the black dashed curve. The open-loop sensitivity at the unstable steady state reaches its maximum value at (a) $v_{max} = 58.17$ and (b) $b = 8.31$.

of the open-loop sensitivity at the unstable steady state is possible for all parameters of the system and can be taken into account as a first step to define a robust bistable behavior. Now, the question is whether the maximization of the open-loop sensitivity at the unstable steady state with respect to parameters is sufficient for minimization of the closed-loop unstable steady state sensitivity to parameters. In the following, we directly measure the unstable steady state sensitivity to the parameters of system (1.4). By comparing the results of the closed-loop to the open-loop sensitivity analysis, we show that maximization of the open-loop sensitivity with respect to parameters is not sufficient in general to minimize the unstable steady state sensitivity. We discuss how we solve this problem by taking into account another important quantity which is the sensitivity of the open-loop response to parameters rather than the input, and formulate a general condition to predict the minimum of unstable steady state sensitivity.

2.2.1 The closed-loop sensitivity analysis: The unstable steady state sensitivity to parameters

We already know that the preservation of unstable steady state against parameter perturbations is key to the maintenance and robustness of bistability. Therefore, we naturally expect that the unstable steady state shows a minimum sensitivity to parameter variations inside the bistability area [88]. We can use the logarithmic sensitivity formula (1.9) to measure the sensitivity of the unstable steady state of system (1.4) to the parameters of the system. For $n = 2$, it

is possible to directly calculate the unstable steady state of system (1.4). Using equation (1.9), the sensitivity of the unstable state P_U to an arbitrary parameter $\alpha \in \Theta$ is defined by

$$S_{P_U}^\alpha(\Theta) = \frac{\alpha}{P_U} \frac{dP_U}{d\alpha}. \quad (2.10)$$

For $\alpha = K_d$, Figure (2.12) illustrates the graph of equation (2.10) as a function of K_d . The diagram shows that the curve is nonmonotone and has a minimum.

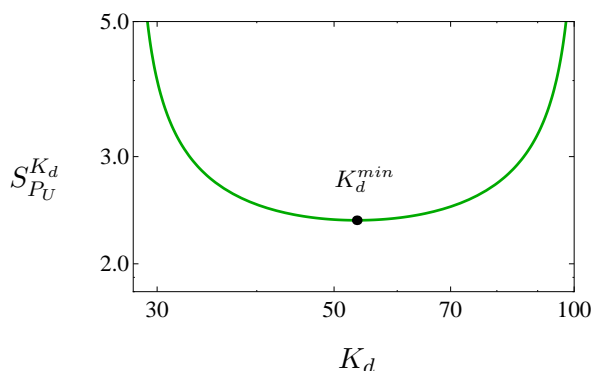


Figure 2.12: The graph of sensitivity of unstable steady state P_U to the parameter K_d for $v_{max} = 200$, $n = 2$, $\gamma = 1$, $b = 1$. The curve is nonmonotone and has a minimum at $K_d = 53.38$. This value is the same as the K_d -value for the maximum of the open-loop sensitivity.

A comparison between Figures (2.10) and (2.12) confirms that the open-loop sensitivity can very well predict the critical value of K_d for which the sensitivity of unstable steady state of the closed-loop system reaches its minimum. This is in fact independent of the selected parameter values in Figures (2.10) and (2.12). The critical value of K_d that both minimizes the closed-loop sensitivity and maximizes the open-loop sensitivity is given by the following equation

$$K_d^{min} = \frac{b^{1/4}}{\gamma} (b + v_{max})^{3/4}. \quad (2.11)$$

Figure (2.13) shows that the maximization of the open-loop sensitivity may not correspond to the minimization of the unstable steady state sensitivity for all parameters of system (1.4). The closed-loop sensitivity to v_{max} and b are calculated using equation (2.10) for $\alpha = v_{max}, b$. The two diagrams depict the existence of minimum for both v_{max} and b . However, these minima are different from the b - and v_{max} -value for the maximum of the open-loop sensitivity. This means that maximization of the open-loop sensitivity alone may not be a sufficient criterion to minimize the unstable steady state sensitivity. In the following, we formulate rigorous mathematical conditions based on the

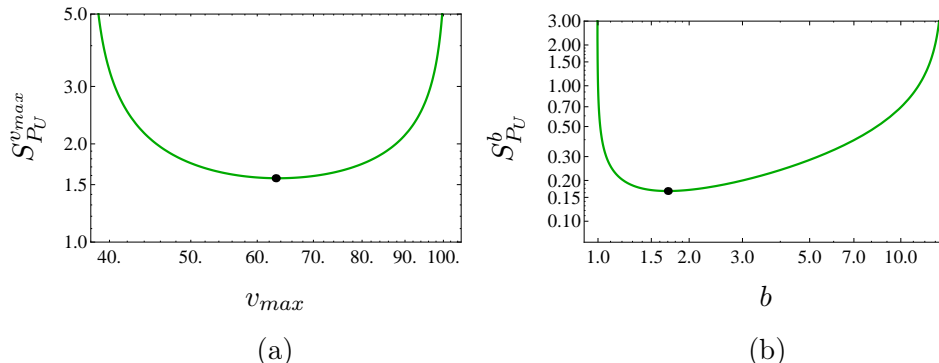


Figure 2.13: The graph of sensitivity of unstable steady state P_U to (a) v_{max} and (b) b for $n = 2$, $\gamma = 1$, and for $b = 1$, $K_d = 20$ in (a) and $v_{max} = 200$, $K_d = 101$ in (b). The sensitivity to these parameters is nonmonotone and has a minimum at $v_{max} = 63.11$ in (a) and at $b = 1.7$ in (b). The b - and v_{max} -values for the minima are not the same as the b - and v_{max} -values for the maxima of the open-loop sensitivity in Figure (2.11).

open-loop sensitivity to predict parameter values for which the unstable steady state sensitivity can be minimized relative to all parameters of a given system like (1.4).

2.2.2 Formulation of the robustness analysis method based on the open-loop sensitivity

We start with a very simple equation that defines the steady states of the closed-loop system; that is,

$$H(\omega, \Theta) := R_\eta(\omega, \Theta) - \omega = 0, \quad (2.12)$$

where $R_\eta(\omega; \Theta)$ is the response of the open-loop system which is defined by equation (1.11) and Θ is the vector of parameters. The unstable steady state satisfies equation (2.12) and as we discussed earlier in Figure (1.10), in a bistable regime, the derivative of the response curve at the unstable steady state is greater than one. This means that

$$\left. \frac{\partial}{\partial \omega} H(\omega; \Theta) \right|_{\omega=P_U} \neq 0. \quad (2.13)$$

According to the implicit function theorem [47], ω can be represented as a function of parameters, in a neighborhood of the unstable steady state P_U . This neighborhood can be expanded as long as we are in the bistability region

in the parameter space. Equation (2.12) can be rewritten as

$$P(\Theta) = R_\eta(\omega; \Theta). \quad (2.14)$$

Taking the logarithmic derivative with respect to an arbitrary parameter $\alpha \in \Theta$ from both sides of equation (2.14) yields

$$S_P^\alpha(\Theta) = \frac{S_\eta^\alpha(\omega; \Theta)}{1 - S_\eta^\omega(\omega; \Theta)}, \quad (2.15)$$

with

$$S_\eta^\alpha(\omega; \Theta) = \frac{\alpha}{R_\eta(\omega; \Theta)} \frac{d}{d\alpha} R_\eta(\omega; \Theta). \quad (2.16)$$

Equation (2.15) is well defined since as stated above, the sensitivity of the response function is greater than one inside the bistability region.

Equation (2.15) establishes the mathematical relationship between the sensitivity of the unstable steady state of the closed-loop system and the sensitivity of the response curve of the open-loop system to the input and the selected parameter α . Given that our goal is to minimize the unstable steady state sensitivity to a parameter, we take the derivative from equation (2.15) with respect to α to get

$$\frac{\partial}{\partial \alpha} \left(\frac{S_\eta^\alpha(\omega; \Theta)}{1 - S_\eta^\omega(\omega; \Theta)} \right) = 0, \quad (2.17)$$

which can be expressed as the following determinant

$$D^\alpha(\omega; \Theta) = \begin{vmatrix} S_\eta^\omega(\omega; \Theta) - 1 & \frac{\partial}{\partial \alpha} S_\eta^\omega(\omega; \Theta) \\ S_\eta^\alpha(\omega; \Theta) & \frac{\partial}{\partial \alpha} S_\eta^\alpha(\omega; \Theta) \end{vmatrix} = 0. \quad (2.18)$$

For every parameter α , equation (2.18) defines a hypersurface in an n -dimensional parameter space, on which the unstable steady state sensitivity takes its minimum with respect to the parameter α . For the sake of simplicity and quick referencing, we call these hypersurfaces α -sensitivity boundaries for each selected α . In Figure (2.14), the α -sensitivity boundaries have been depicted for $\alpha = v_{max}, b, K_d$ in a two-dimensional space. Instead of focusing on each α -sensitivity boundary and trying to minimize the unstable steady state sensitivity to α , we are interested to explore regions inside the bistability area in which the unstable steady state sensitivity can be minimized relative to all parameters of the system. The b -sensitivity and v_{max} -sensitivity boundaries, determined by upper and lower dashed curves, enclose a region inside the bistability area in

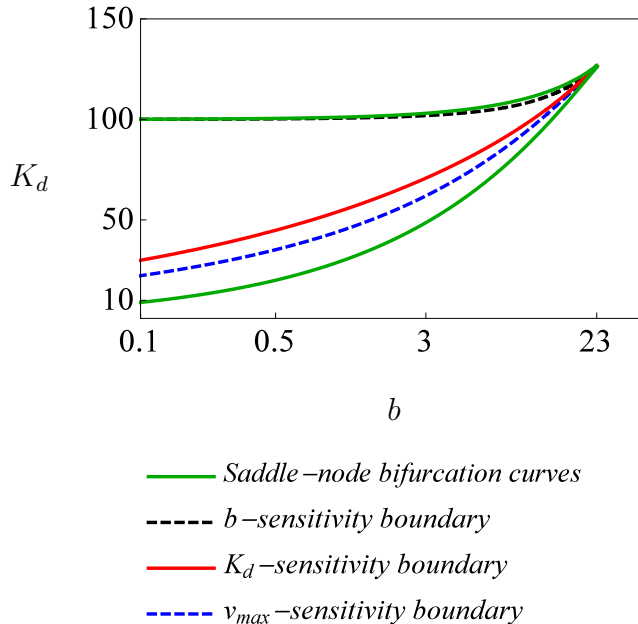


Figure 2.14: Bifurcation diagram of system (1.4) for $v_{max} = 200$, $n = 2$ and $\gamma = 1$. The K_d -sensitivity boundary yields the parameter values for a robust bistable behavior in the system.

which there is possibility for the unstable steady state sensitivity to be minimized relative to these two parameters. The K_d -sensitivity boundary gives us the best position inside this region in which the unstable steady state sensitivity can be minimized relative to three parameters. In fact, the K_d -sensitivity boundary defines the most inner region bounded by the α -sensitivity boundaries. We refer to this region as the robust bistability region. It should be noted that the robust bistability region is not always a curve. Later, we will study other example systems of higher dimensions for which the robust bistability region is a two-dimensional region. We should also note that the γ -sensitivity boundary is exactly the same as the K_d -sensitivity boundary and therefore, it is not mentioned in the figure. Ma & Iglesias [51] had previously proposed a measure of robustness in a one-dimensional parameter space. The measure considers the proximity of a nominal parameter value to the boundaries of a parameter interval in which a dynamical characteristic like bistability emerges. This measure is called the degree of robustness and is defined as follows

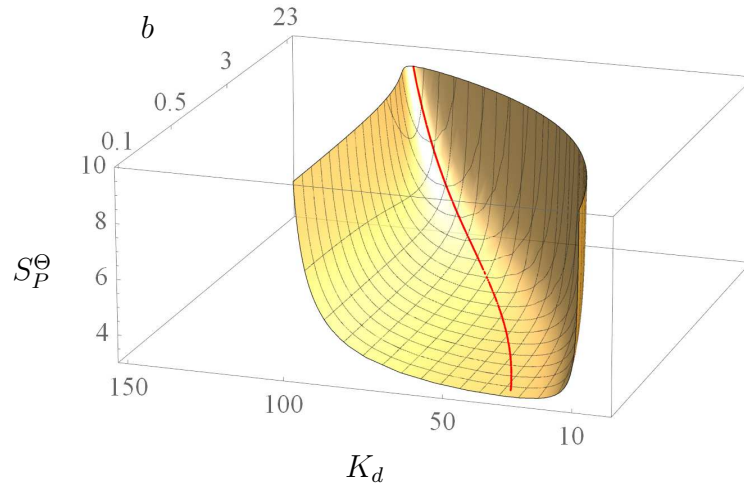
$$DOR = 1 - \max\left\{\frac{k_l}{k}, \frac{k}{k_u}\right\}, \quad (2.19)$$

where $k \in (k_l, k_u)$ is the nominal value and k_l and k_u are the bifurcation values. Equation (2.19) always gives a value between 0 and 1 for different choices of the nominal parameter value k . If the value is close to zero, the system is very sensitive to the parameter value, but for values close to one, system is insensitive and as a result robust to the chosen parameter value. For every fixed b in Figure (2.14), it is interesting to see that our predicted value of K_d maximizes the degree of robustness (2.19).

To further validate that on the K_d -sensitivity boundary the unstable steady state sensitivity can be minimized relative to all parameters of system (1.4), we calculate the cumulative sensitivity [88] that gives a measure for the total sensitivity to all parameters of the system and is defined by

$$S_P^\Theta(\Theta) = |S_P^b(\Theta)| + |S_P^{v_{max}}(\Theta)| + |S_P^{K_d}(\Theta)|, \quad (2.20)$$

where $S_P^\alpha(\Theta)$, $\alpha = b, v_{max}, K_d$, is calculated in an open-loop setting by using equation (2.15). The cumulative sensitivity is a good measure to evaluate the total sensitivity of the unstable steady state to all parameters of a system. The graph of equation (2.20) is plotted in Figure (2.15). As illustrated in the figure,



— K_d -sensitivity boundary

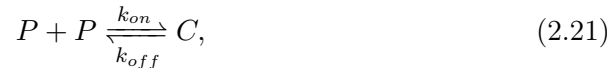
Figure 2.15: Cumulative sensitivity manifold for system (1.4). The manifold takes its minimum along the K_d -sensitivity boundary.

the cumulative sensitivity takes its minimum along the K_d -sensitivity boundary for different values of b and K_d in the bifurcation diagram (2.14). Figure (2.15)

confirms that the total sensitivity of the unstable steady state to all parameters can be minimized on the K_d -sensitivity boundary. Therefore, we can already expect that on this curve, parameter perturbations have the least effect on the bistability. Our results also reveal that in the set of parameters of system (1.4), K_d is a key parameter for creating robust bistability in the system.

2.2.3 One-gene positive feedback loop with protein homodimerization

Molecular homodimerization is a mechanism through which two identical molecules bind and form a complex. The complex is called a dimer molecule. In the field of molecular biology, binding of two inactive identical proteins can form an active protein that can for example act as a transcription factor. For a protein like P , the homodimerization is expressed by the following simple chemical equation



where P can be considered as an inactive protein and C can be taken as an active complex. The two parameters k_{on} and k_{off} are the association and dissociation rate constants, respectively. Based on the law of mass action [75, 76], differential equations that model this mechanism read as follows

$$\begin{aligned} \dot{P} &= -2k_{on}P^2 + 2k_{off}C, \\ \dot{C} &= k_{on}P^2 - k_{off}C. \end{aligned} \quad (2.22)$$

It is assumed in system (2.22) that there is no production and degradation for the chemical components. Under this assumption, system (2.22) becomes a closed chemical system in which all concentrations are conserved. In fact, the following mathematical relation holds between the two equations of system (2.22)

$$\dot{P} + 2\dot{C} = 0, \quad (2.23)$$

which in turn yields

$$P + 2C = P_T, \quad (2.24)$$

where P_T is the total concentration of protein P . Putting system (2.22) at the steady state and applying equation (2.24), we get

$$P = \frac{1}{4} \left(-\kappa_d + \sqrt{\kappa_d^2 + 8P_T\kappa_d} \right). \quad (2.25)$$

Equation (2.25) expresses the free concentration P as a function of the total concentration P_T . The parameter $\kappa_d = \frac{k_{off}}{k_{on}}$ is the equilibrium dissociation constant of the protein-protein binding. It is discussed in [16] that homodimerization is capable of creating ultrasensitivity. This ultrasensitivity is much weaker than that of created by molecular titration. However, as we will see, it can bring about bistability in a one-gene positive feedback system even in the absence of molecular cooperativity. The graph of equation (2.25) is illustrated in Figure (2.16) for selected values of κ_d . Different values of κ_d represent

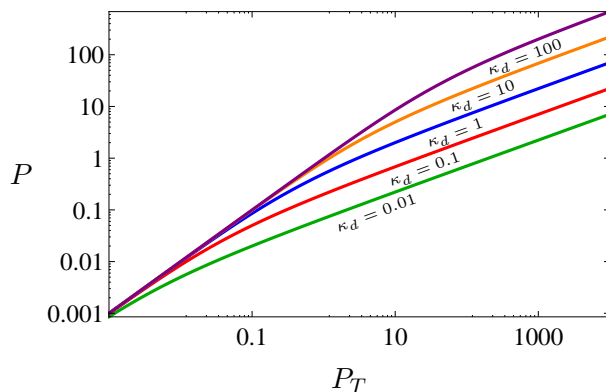


Figure 2.16: Plot of concentration of free protein P as a function of its total concentration P_T for different values of κ_d . For $P_T < \kappa_d$, the response curves exhibit ultrasensitivity.

different homodimerization strengths; the lower the value of this parameter is, the stronger the mechanism will be. According to Figure (2.16), equation (2.25) exhibits ultrasensitivity for $P_T < \kappa_d$.

Now, we assume that P as a transcription factor dimerizes to form the active complex C that can bind a promoter and induce the gene transcription. We assume that the promoter region has only one binding site so that the possibility of a cooperative binding to promoter is ruled out and ultrasensitivity is created solely by the homodimerization mechanism. Figure (2.17) depicts a schematic diagram of the system. The system is expressed by the following set of differential equation

$$\begin{aligned} \dot{P} &= b_P + v_{max} \frac{C}{K_d + C} - 2k_{on}P^2 + 2k_{off}C - \gamma_P P, \\ \dot{C} &= k_{on}P^2 - k_{off}C - \gamma_C C, \end{aligned} \quad (2.26)$$

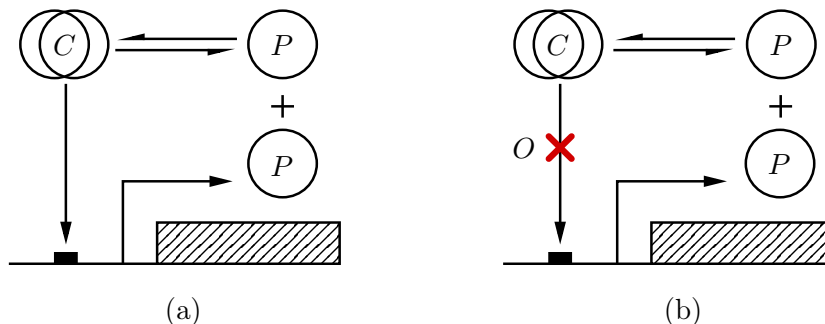


Figure 2.17: A one-gene positive feedback loop with the homodimerization mechanism. (a) The closed-loop system. (b) The open-loop system with the opening point O .

where b_P is the basal and v_{max} is the maximum production rates, K_d is the equilibrium dissociation constant of the protein-promoter binding, and γ_P and γ_C are the degradation rate constants of the monomer and dimer proteins. It is straightforward to show the existence of bistability in system (2.26). We get the steady state equation

$$A_4(\Theta)P^4 + A_3(\Theta)P^3 + A_2(\Theta)P^2 + A_1(\Theta)P + A_0(\Theta) = 0, \quad (2.27)$$

where Θ is the vector of all parameters with a new lumped parameter defined as

$$\kappa_d = \frac{k_{off} + \gamma_C}{k_{on}}. \quad (2.28)$$

We can think of κ_d as the protein-protein equilibrium dissociation constant. Bifurcation diagram of system (2.26) is illustrated in Figure (2.18) in the (κ_d, K_d) -space. The two saddle-node bifurcation boundaries intersect at the cusp bifurcation point C . The bistability region in Figure (2.18) provides interesting information on how parameters interact to bring about bistability in system (2.26). Since the homodimerization mechanism is part of the positive feedback loop, both K_d and κ_d can be considered as measures of the positive feedback strength and its effect on bistability. This role is more pronounced for κ_d because the Hill number in equation (2.26) is one and therefore, in the absence of cooperativity, the necessary ultrasensitivity for bistability is created by the homodimerization mechanism. The bifurcation diagram shows very well how the two dissociation constants interact with each other in a bistable regime; the higher values of K_d are compensated by lower values of κ_d and vice versa. In other words, when the protein-promoter binding is not strong (high K_d), a very strong homodimerization effect (low κ_d) can create a large concentration of dimer proteins so that

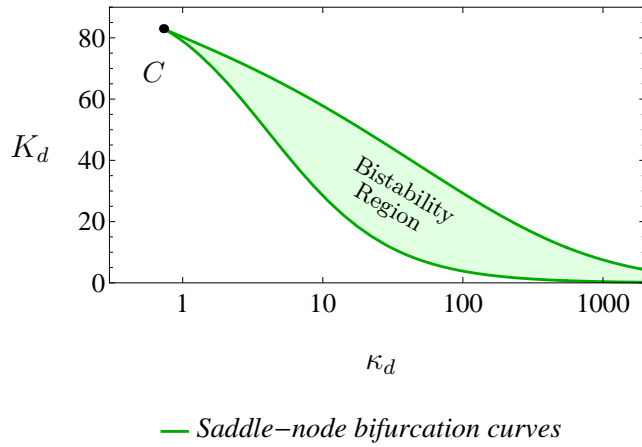


Figure 2.18: Bifurcation diagram of system (2.26) for $v_{max} = 200$, $\gamma_P = 1$, $\gamma_C = 1$ and $b_P = 0.5$. The intersection of saddle-node bifurcation curves defines a cup bifurcation point at C .

the resulting positive feedback strength can maintain the bistable behavior. On the other side of the bifurcation diagram, for weak protein-protein binding (high κ_d), bistability will be preserved as a result of strong protein-promoter binding (low K_d) when the dimer protein is available at low concentrations. It is also clear from the bifurcation diagram that the bistability range of κ_d is quite larger than K_d meaning that the homodimerization process has a key role in creating and maintaining bistability in system (2.26).

In order to look for the robust bistability region inside the bistability area (2.18), we first open the positive feedback loop as shown in Figure (2.17:b). The corresponding open-loop equations are

$$\begin{aligned} \dot{P} &= b_P + v_{max} \frac{\omega}{K_d + \omega} - 2k_{on}P^2 + 2k_{off}C - \gamma_P P, \\ \dot{C} &= k_{on}P^2 - k_{off}C - \gamma_C C, \end{aligned} \quad (2.29)$$

with ω as the constant input and all the other C 's as the output. The steady state input-output response of system (2.29) is achieved by solving the following equation

$$b_P - 2\gamma_C C - \sqrt{\kappa_d C} + v_{max} \frac{\omega}{K_d + \omega} = 0. \quad (2.30)$$

The solution of equation (2.30) is not unique and there are two positive solutions for C as a function of ω . A simple biological consideration will help us pick the right solution; by putting both ω and b_P equal to zero, only one of the solutions become zero, which means that if the monomer is not produced,

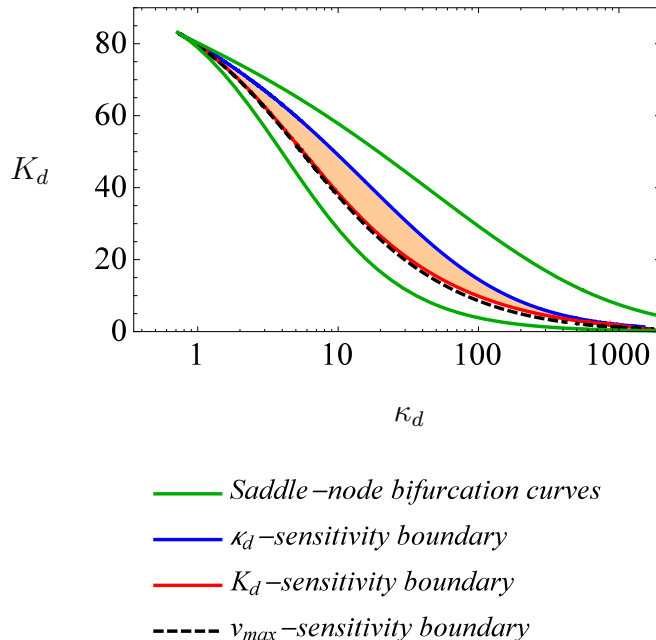


Figure 2.19: Bifurcation diagram of system (2.26) for $v_{max} = 200$, $\gamma_P = 1$, $\gamma_C = 1$ and $b_P = 0.5$. The robust bistability region is illustrated by the shaded area. Those sensitivity boundaries which are not shown in the figure, lie on either the saddle-node bifurcation curves or the existing sensitivity boundaries.

there will be no dimer proteins. Having solved equation (2.30) for C , we can obtain the open-loop sensitivity to the input and to each parameter and calculate the determinant (2.18). The resulting boundaries for different parameters of systems (2.29) are shown in Figure (2.19). We again focus on the most inner region defined by the boundaries. This region is shaded in the figure. Inside the shaded region, we expect to have the minimum of unstable steady state sensitivity relative to all parameters of the system. Those parameter sensitivity boundaries which are not shown in Figure (2.19) lie on either the saddle-node bifurcation curves or the existing boundaries. It is interesting to see that the robust bistability region is enclosed by the K_d - and κ_d -sensitivity boundaries. This again confirms that for a robust bistable behavior in system (2.26), K_d and κ_d have a decisive role in the parameter space. The cumulative sensitivity S_C^Θ also shows that the total sensitivity of the unstable steady state to all parameters takes its minimum inside the robust bistability region. The manifold of cumulative sensitivity is depicted in Figure (2.20).

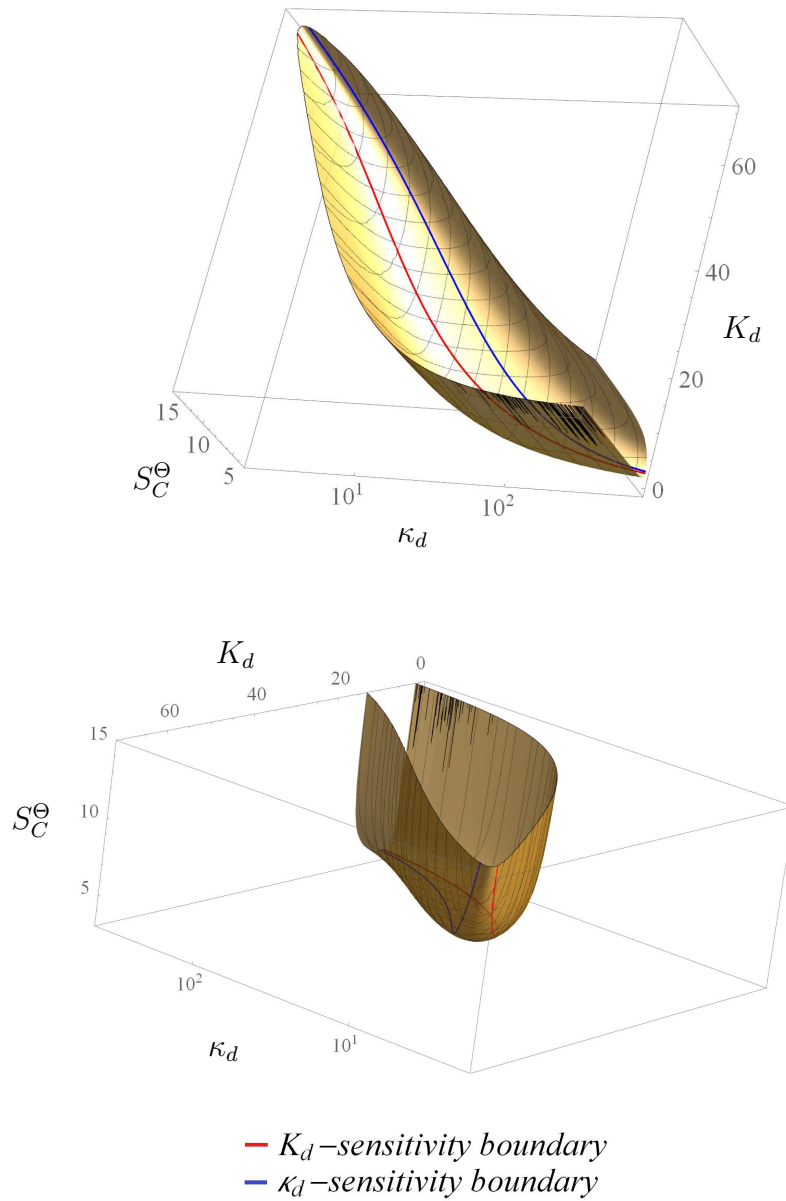
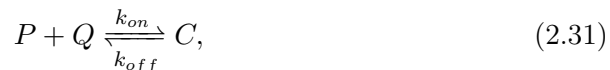


Figure 2.20: Cumulative sensitivity manifold for system (2.26). The manifold takes its minimum inside the robust bistability region.

2.2.4 One-gene positive feedback loop with molecular titration

Molecular titration or sequestration is a process in which two nonidentical molecules bind to form a complex molecule which is called a heterodimer. In molecular biology, an inhibitor protein titrates an active protein into an inactive complex so that the active protein loses its function. For two proteins like P and Q , titration is illustrated by the following simple chemical equation



where P is the active protein, Q is the inhibitor protein and C is the inactive complex. We can set up differential equations for the chemical system (2.31) as follows

$$\begin{aligned} \dot{P} &= -k_{on}PQ + k_{off}C, \\ \dot{Q} &= -k_{on}PQ + k_{off}C, \\ \dot{C} &= k_{on}PQ - k_{off}C. \end{aligned} \quad (2.32)$$

We assume that different components are neither produced nor degraded. Based on the conservation of matter, we have

$$P + C = P_T \quad \text{and} \quad Q + C = Q_T, \quad (2.33)$$

where P_T and Q_T are the total concentrations of P and Q respectively. Taking equations (2.33) into account, the steady state value of the active protein P is given by

$$P = \frac{1}{2} \left(P_T - Q_T - K_d + \sqrt{(P_T - Q_T - K_d)^2 + 4P_T K_d} \right), \quad (2.34)$$

with $\kappa_d = \frac{k_{off}}{k_{on}}$ as the equilibrium dissociation constant of the protein-protein binding. Equation (2.34) expresses the free concentration P as a function of total concentrations P_T and Q_T . As discussed in [16], molecular titration can generate ultrasensitive responses equivalent to highly cooperative processes. Figure (2.21) depicts the logarithmic plot of equation (2.34) for different total concentrations of the inhibitor. According to Figure (2.21), the more the inhibitor concentration is, the stronger the buffering and ultrasensitivity will be. It is discussed in [16] that strong buffering and ultrasensitivity happen when

$$\frac{Q_T}{\kappa_d} > 1. \quad (2.35)$$

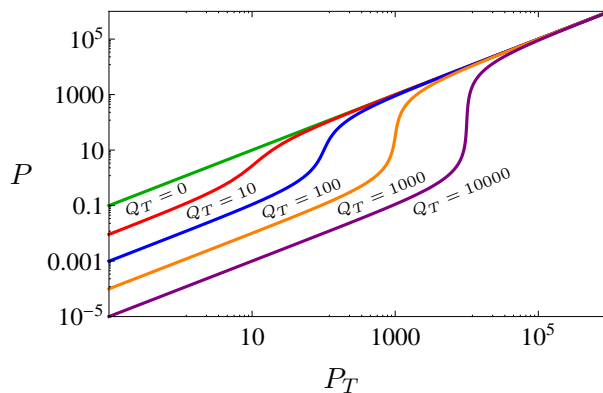


Figure 2.21: Plot of concentration of free protein P as a function of its total concentration P_T for $\kappa_d = 1$ and different values of Q_T . For higher concentrations of protein Q the response curves exhibit stronger buffering and higher ultrasensitivity. The buffering of protein P happens when $P_T < Q_T$ and the ultrasensitivity is generated at the threshold $P_T \approx Q_T$.

The ratio in inequality (2.35) is called the stoichiometric binding constant. In Figure (2.21), all the response curves exhibit ultrasensitivity at the threshold defined by $P_T \approx Q_T$.

The protein P in reaction (2.31) can also be taken as an active transcription factor which can bind to a promoter and initiate transcription of a gene sequence into an mRNA strain. It is shown that sequestration of an active transcription factor by an inhibitor can convert a graded transcriptional response into an ultrasensitive binary response [15] which is necessary for the emergence of bistability in feedback systems. We suppose that a protein like Q can bind P and inhibit transcription by forming an inactive complex. The process has been schematically shown in Figure (2.22). The system is expressed by the following set of different equations

$$\begin{aligned}
 \dot{P} &= b_P + v_{max} \frac{P}{K_d + P} - k_{on}PQ + k_{off}C - \gamma_P P, \\
 \dot{Q} &= b_Q - k_{on}PQ + k_{off}C - \gamma_Q Q, \\
 \dot{C} &= k_{on}PQ - k_{off}C - \gamma_C C,
 \end{aligned} \tag{2.36}$$

where b_P and b_Q are the basal expression rates for the activator P and the inhibitor Q respectively, v_{max} is the maximum production rate, K_d is the equilibrium dissociation constant of the protein-promoter binding, and γ_P , γ_Q and γ_C are the degradation rate constants of activator, inhibitor and complex proteins. The steady state equation of the closed-loop system (2.36) takes the

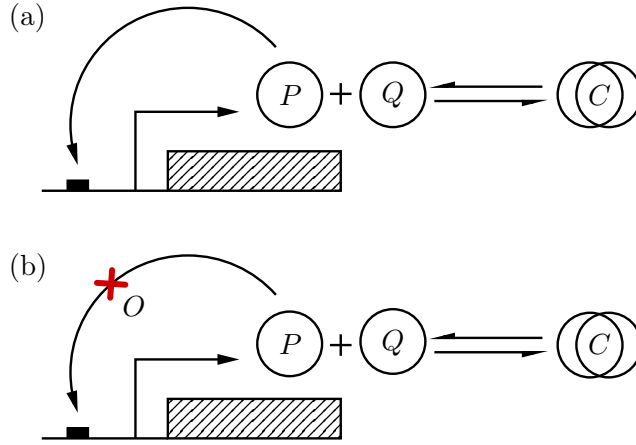


Figure 2.22: A one-gene positive feedback loop with the molecular titration mechanism. (a) The closed-loop system. (b) The open-loop system with the opening point O .

following form

$$A_3(\Theta)P^3 + A_2(\Theta)P^2 + A_1(\Theta)P + A_0(\Theta) = 0, \quad (2.37)$$

where Θ is the vector of all parameters with a new lumped parameter defined as

$$\kappa_d = \frac{\gamma P \gamma Q}{\gamma C} \left(\frac{k_{off} + \gamma C}{k_{on}} \right). \quad (2.38)$$

Just like equation (2.28), the parameter κ_d in the above equation can be considered as the protein-protein equilibrium dissociation constant. We earlier discussed that in system (2.26), the homodimerization process is part of the positive feedback loop. Therefore, interaction of the two parameters K_d and κ_d can very well illustrate how homodimerization as an ultrasensitive mechanism can create bistability together with a positive feedback loop. In system (2.36), however, the titration mechanism is not part of the feedback loop and has an external influence on the positive feedback loop. It should also be noted that, just like system (2.26), there is no cooperativity in system (2.36) and the necessary ultrasensitivity for bistability is solely created by the titration mechanism. According to the above discussions, we can separate the role of parameters based on the two distinct parts of the system, that is, the positive feedback loop which positively contribute to the dynamics of the system and the titration part which negatively regulates the system. The parameter K_d represents the strength of the feedback loop as it measures the strength of protein-promoter binding. For the titration mechanism, the two parameters κ_d and b_Q can be used as a measure of

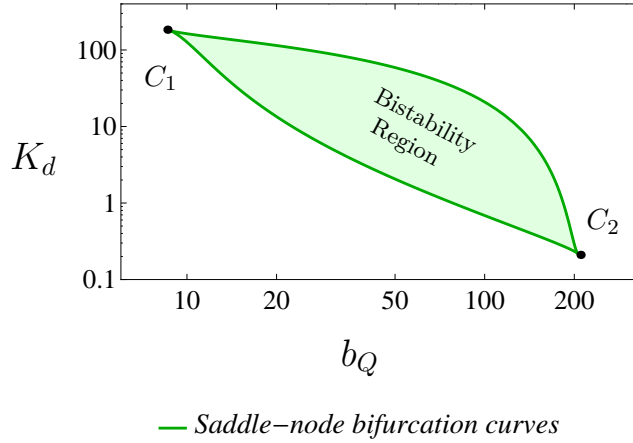


Figure 2.23: Bifurcation diagram of system (2.36) for $v_{max} = 200$, $\gamma_P = \gamma_C = \gamma_Q = 1$, $\kappa_d = 0.2$ and $b_P = 8$. The two saddle-node bifurcation curves intersect at two cusp points C_1 and C_2 .

titration strength; b_Q determines the level of inhibitor protein and κ_d defines the strength of activator protein sequestration by the inhibitor protein. Any bifurcation diagram that gives the bistability region in a parameter space consisting of K_d and either κ_d or b_Q , can very well illustrate how titration mechanism and the positive feedback loop can create bistability in system (2.36). Bifurcation diagram of system (2.36) is illustrated in Figure (2.23) in the (b_Q, K_d) -space. In this parameter space, the two saddle-node bifurcation boundaries intersect at two cusp bifurcation points C_1 and C_2 . The two cusp points determine the maximum parameter ranges for bistability; for high values of K_d (weak positive feedback effect), the level of inhibitor has to be low (low b_Q) for the system to undergo bistability, while high values of b_Q (strong titration effect) are compensated with low values of K_d (strong feedback effect). This shows that the titration mechanism as a negative regulatory motif and the positive feedback loop have opposing effects at the two extreme parameter ranges. However, in the middle ranges, the two opposing effects get very balanced to bring about a relatively broad parameter range for bistability. We can now look for the robust bistability region inside the bistability area (2.23). For this, we open the positive feedback loop as shown in Figure (2.22:b). The corresponding open-loop equations are

$$\begin{aligned}
 \dot{P} &= b_P + v_{max} \frac{\omega}{K_d + \omega} - k_{on}PQ + k_{off}C - \gamma_P P, \\
 \dot{Q} &= b_Q - k_{on}PQ + k_{off}C - \gamma_Q Q, \\
 \dot{C} &= k_{on}PQ - k_{off}C - \gamma_C C,
 \end{aligned} \tag{2.39}$$

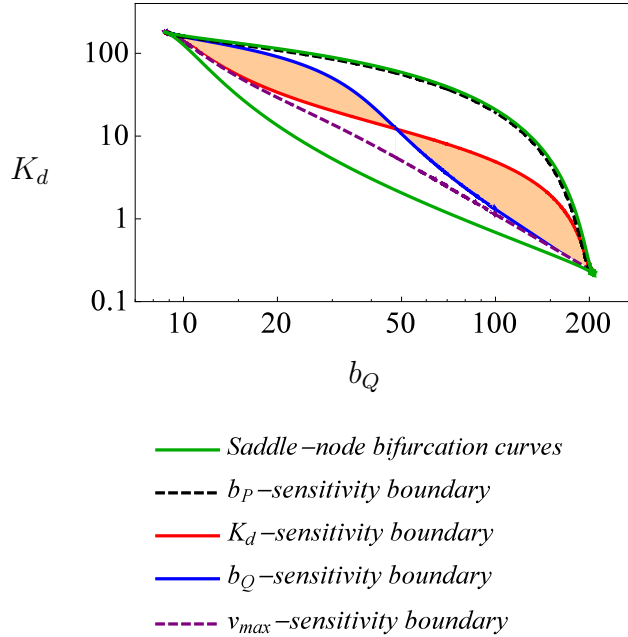


Figure 2.24: Bifurcation diagram of system (2.36) for $v_{max} = 200$, $\gamma_P = 1$, $\gamma_C = 1$ and $b_P = 0.5$. The robust bistability region is illustrated by the shaded area. Those parameter sensitivity boundaries which are not shown in the figure, lie on either the saddle-node bifurcation curves or the existing boundaries.

with ω as the constant input and all the other P 's as the output. The steady state input-output response of system (2.39) is achieved by solving the following equation

$$-\gamma_P P^2 + \left(v_{max} \frac{\omega}{K_d + \omega} + b_P - b_Q - \kappa \right) P + \frac{\kappa}{\gamma_P} \left(v_{max} \frac{\omega}{K_d + \omega} + b_P \right) = 0. \quad (2.40)$$

Solution of equation (2.40) can be used to calculate the determinant (2.18) for parameters of the system. The resulting boundaries for different parameters of system (2.39) are shown in Figure (2.24). The most inner region is enclosed by the b_Q - and K_d -sensitivity boundaries which is shown by the shaded area. Again, those parameter sensitivity boundaries which are not illustrated in the figure, lie on either the saddle-node bifurcation curves or the existing sensitivity boundaries. The enclosure of the robust bistability region by the b_Q - and K_d -sensitivity boundaries shows the significance of these two parameters in creating robust bistability in system (2.36). The parameter K_d regulates the strength of the positive feedback loop and b_Q controls the level of ultrasensitivity that is created by the titration mechanism. We can also see in Figure (2.25) that the cumulative sensitivity S_P^Θ of the unstable steady state takes its minimum inside the robust bistability region which approves the fact that the total sensitivity

of the unstable steady state to all parameters can be minimized in the robust bistability region.

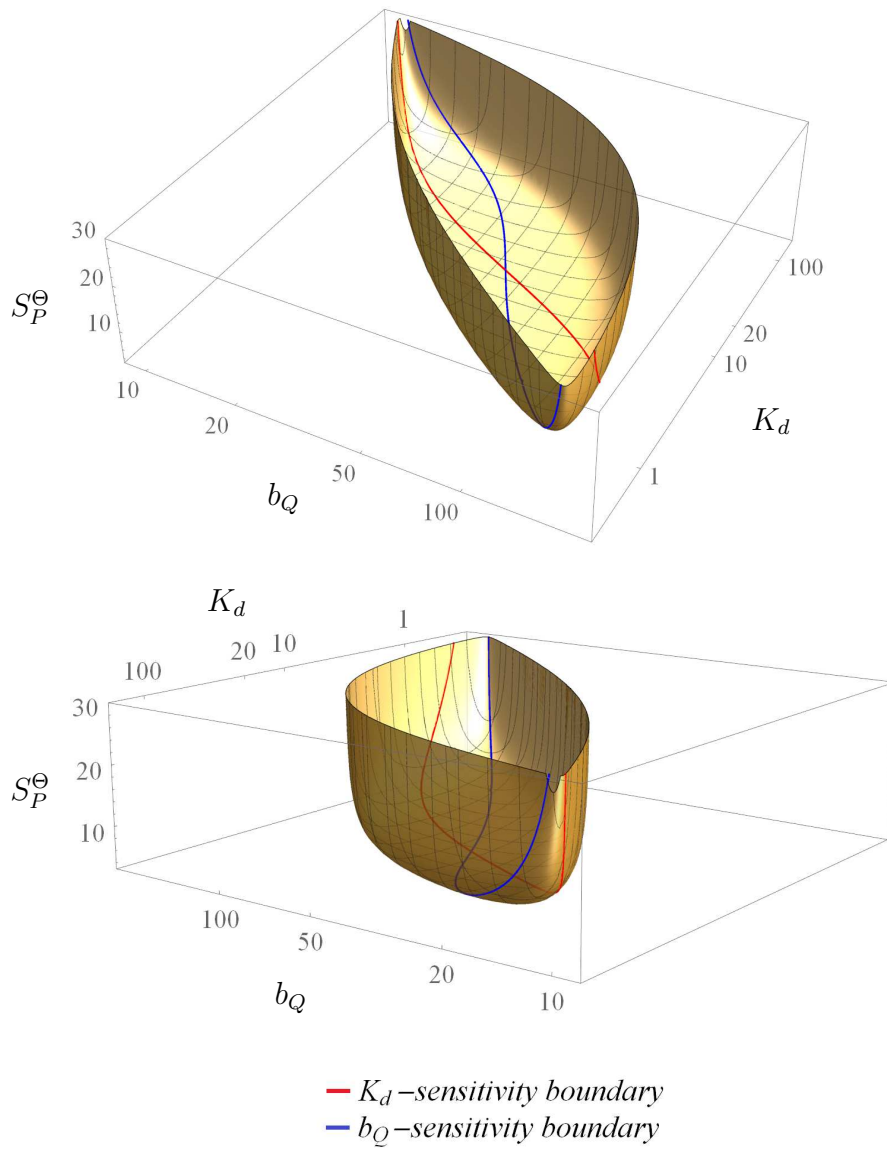


Figure 2.25: Cumulative sensitivity manifold for system (2.36). The manifold takes its minimum inside the robust bistability region.

2.3 The *GAL* network

The galactose metabolic network in *Saccharomyces cerevisiae*, *GAL* network for short, is a well-known genetic switch that has been long recognized for studying a variety of molecular mechanisms like protein-protein and protein-DNA interactions. In the absence of glucose as the main energy source, the *GAL* network metabolizes galactose through Leloir metabolic pathway [13]. The pathway performs under the regulation of a set of regulatory proteins and enzymes that define altogether the *GAL* network. Over the past decades, extensive mathematical studies have been carried out on the *GAL* network to investigate the emergence of the bistable switch [1, 6, 19, 93].

The *GAL* network consists of three regulatory genes, *GAL4*, *GAL80*, and *GAL3* and five structural genes, *GAL1*, *GAL2*, *GAL7*, *GAL10*, which enable the network to metabolize galactose [69]. The regulatory gene *GAL4* encodes the protein Gal4p that acts as a transcription factor. This protein initiates the transcription of *GAL* genes by binding to their upstream activation sequences (UASG) [28]. The regulatory genes *GAL3* and *GAL80* have one binding site on their promoter while the structural genes have multiple binding sites on their promoter; *GAL2* and *GAL7* have two binding sites, whereas *GAL1* and *GAL10* have four shared binding sites. The *GAL80* gene encodes the protein Gal80p that acts as a repressor of the transcription in *GAL* network. This protein binds the Gal4p on the DNA and represses the active promoter [54]. The *GAL3* and *GAL1* genes encode proteins Gal3p and Gal1p that in the presence of galactose in the media can interact with Gal80p and remove its repression by binding the Gal80p protein [6, 69]. The function of proteins Gal80p, Gal3p and Gal1p leads to the emergence of the three important feedback loops in the *GAL* network, namely, a negative feedback loop which is defined by the Gal80p repression of the activator Gal4p, and two positive feedback loops through the Gal3p and Gal1p repression of Gal80p protein [70].

In this section, we are going to study the role of three important proteins of the *GAL* network in creating bistability in this network. Bistability is an important dynamical characteristic in *Saccharomyces cerevisiae* since it creates a persistent memory of the energy source that the network finds in the environment [1]. We investigate the emergence of bistability by developing a mathematical model that includes all protein-protein as well as protein-DNA interactions. We construct our model step by step by studying three layers of the network. These layers are created by isolating the activity of each of the proteins by deleting

the other genes. We perform nonlinear regression on the experimental data to estimate the parameter values of our model. We also discuss in detail the role of homodimerization and titration in modeling the bistability in the *GAL* network. We start with the first layer of the network.

2.3.1 The 1st layer of the galactose network: Gal4p decay data

In the first layer of the *GAL* network, the activity of Gal4p is isolated by deleting the *GAL80* gene. In the absence of Gal80p protein, the transcription factor Gal4p can activate the transcription of other genes without being repressed by Gal80p. Therefore, we can calculate the protein-protein and protein-DNA binding affinities for Gal4p. In order to control variations in the level of Gal4p, the endogenous promoter of *GAL4* has been replaced with a doxycycline repressible system. After the full activation of the system, the production of *GAL4* mRNA will be stopped and it can only be produced at the basal level. Shutting off the *GAL4* mRNA production helps measure the decay of Gal4p protein over time.

2.3.1.1 Gal4p decay process in galactose

The experimental data for the Gal4p decay process is given in Table (2.1) which present the reduction in the total concentration of Gal4p protein over time. The data in Table (2.1) is obtained after shutting off the *GAL4* mRNA production at time zero. At this stage, *GAL4* mRNA is produced at a basal level.

| Time (h) | <i>Gal4_{PT}</i> in galactose (N) |
|----------|---|
| 0 | 993.24 |
| 1.5 | 534.23 |
| 3 | 294.34 |
| 4.5 | 161.32 |
| 6 | 99.52 |
| 7.5 | 59.34 |
| 9 | 41.23 |
| 10.5 | 39.45 |
| 12 | 40.43 |

Table 2.1: Total concentration of Gal4p protein (*Gal4_{PT}*) in galactose medium for different time points.

The explained production and decay processes for the total concentration of

Gal4p protein is simply modeled by the following differential equation

$$\frac{d}{dt}Gal4_{PT}(t) = b_{G4} - \gamma_{G4}Gal4_{PT}(t), \quad (2.41)$$

with the initial condition

$$Gal4_{PT}(0) = Gal4_0. \quad (2.42)$$

The total concentration of Gal4p protein is represented by $Gal4_{PT}$, b_{G4} denotes the basal expression rate and γ_{G4} is the decay rate constant. The ultimate goal of our decay process investigation is to find the decay rate constant by using the nonlinear regression. Equation (2.41) is a first order differential equation and its exact solution is given by the following equation

$$Gal4_{PT}(t) = Y + Ae^{Rt}, \quad (2.43)$$

where

$$R = -\gamma_{G4}, \quad A = Gal4_0 - \frac{b_{G4}}{\gamma_{G4}}, \quad Y = \frac{b_{G4}}{\gamma_{G4}}. \quad (2.44)$$

We perform the nonlinear regression to fit equation (2.43) to the data in Table (2.1). The Result of nonlinear regression is illustrated in Figure (2.26). The

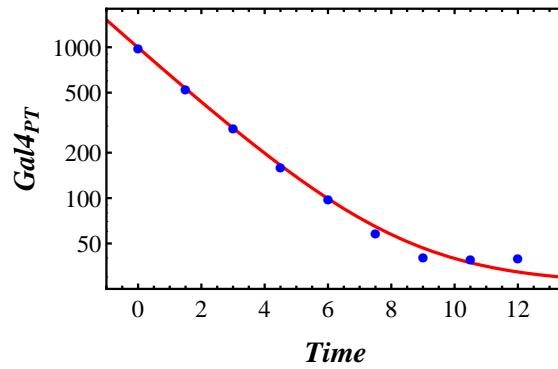


Figure 2.26: The result of nonlinear regression for total concentration of Gal4p protein in galactose medium using equation (2.43). The nonlinear data fit predicts that Gal4p has a half-life of 1.61 hours.

parameter estimates with the corresponding standard errors and confidence intervals are given in Table (2.2). The numbers in the table suggest that the results of the nonlinear regression are reasonably good and reliable. According

to the table and equation (2.43), the decay rate constant will be

$$\gamma_{G4} = 0.43 h^{-1}, \quad (2.45)$$

which is equivalent to the half-life of 1.61 hours. This is biologically reasonable because the half-life of a protein is between 1 – 2 hours.

| Parameter | Estimate | Standard Error | Confidence Interval |
|-----------|----------|----------------|---------------------|
| Y | 26.98 | 3.01 | (19.63, 34.34) |
| A | 967.28 | 5.4 | (954.05, 980.51) |
| R | 0.43 | 0.005 | (0.41, 0.44) |

Table 2.2: Parameter estimates and the corresponding standard errors and confidence intervals for equation (2.43) and the data set (2.1).

Moreover, the basal expression rate is given as follows

$$b_{G4} = 11.6 Nh^{-1}. \quad (2.46)$$

Now that the decay rate constant for the total Gal4p protein is calculated, we can investigate the interaction of Gal4p protein with other genes' promoters. We study the regulatory role of Gal4p protein on two promoters *GAL7* and *GCY1* by analyzing the mRNA level of each promoter as a function of Gal4p total concentration.

2.3.1.2 The regulatory effect of Gal4p protein on the *GAL7/GCY1* promoter response

As mentioned in the previous section, in the absence of Gal80p which acts as an inhibitor, Gal4p can freely activate the transcription of genes whose promoters are regulated by this protein. We study the mRNA level of two genes; the first one is *GAL7* whose promoter has two binding sites and the second one is *GCY1* whose promoter has only one binding site for Gal4p protein. These two examples provide a very good framework for the study of Gal4p effect on the level of these genes' mRNA since in the case of *GAL7* we can expect cooperativity among Gal4p proteins to bind the promoter, while in the case of *GCY1* there is no such possibility. As we will show in the following, this fact can help us identify the nonlinear processes that are involved in the system and have to be considered in our mathematical modeling. We start with a simple Hill function as a first step in building our model.

Fitting the Hill function

As explained in the previous chapters, Hill function as a sigmoidal function can very well express the switch-like responses in gene networks. In this section, we are going to fit a Hill function to *GAL7/GCY1* mRNA data that models the changes in the level of mRNA as a function of total concentration of Gal4p. Table (2.3) gives the total concentration of Gal4p and the corresponding *GAL7* and *GCY1* mRNA levels in galactose medium.

The data in Table (2.3) show that as the Gal4p decays, the production of mRNA diminishes since the level of transcription factor goes down exponentially. Experimentally speaking, the interesting point about the data in Table (2.3) is that it can facilitate the study of both Gal4p decay and Gal4p-promoter binding processes with just one round of experimental measurement. In using a Hill function as our model, we assume that only Gal4p monomers bind *GAL7/GCY1* promoters to induce the gene transcription. The mRNA dynamics simply read as follows

$$\frac{d}{dt}M = b_M + v_M \frac{Gal4_{PF}^n}{K_d^n + Gal4_{PF}^n} - \gamma_M M, \quad (2.47)$$

where M represents the concentration of mRNA (either *GAL7* or *GCY1*), b_M is the basal expression rate, v_M defines the maximum level of promoter activity, K_d is the equilibrium dissociation constant for Gal4p-promoter binding, γ_M is the decay rate of the mRNA, and finally, $Gal4_{PF}$ denotes the free concentration of Gal4p protein.

| <i>Gal4_{PT}</i> (N) | <i>GAL7</i> mRNA (N) | <i>GCY1</i> mRNA (N) |
|------------------------------|----------------------|----------------------|
| 993.24 | 1.38 | 0.53 |
| 534.23 | 1.18 | 0.4 |
| 294.34 | 0.96 | 0.31 |
| 161.32 | 0.54 | 0.18 |
| 99.5 | 0.18 | 0.009 |
| 59.34 | 0.04 | 0.05 |
| 41.23 | 0.01 | 0.04 |
| 39.45 | 0.01 | 0.037 |
| 40.43 | 0.008 | 0.03 |

Table 2.3: Total concentration of Gal4p protein in galactose medium with the corresponding *GAL7/GCY1* mRNA levels.

At the steady state, equation (2.47) can be solved for M to yield the following equation

$$M = B + V \frac{Gal4_{PF}^n}{K_d^n + Gal4_{PF}^n}, \quad (2.48)$$

where $B = b_M/\gamma_M$ and $V = v_M/\gamma_M$. Equation (2.48) describes an input-output response of a promoter as a function of Gal4p protein. It is worth noting again that since there are no Gal80p in the first layer, the total concentration of Gal4p freely interacts with the promoters; therefore, we take

$$Gal4_{PF} = Gal4_{PT}, \quad (2.49)$$

in equation (2.48). In order to estimate the parameter values in equation (2.48), we perform the nonlinear regression to fit this equation to the mRNA data. We fix the values of V and B based on the highest and lowest levels of mRNA in Table (2.3). The results are illustrated in Figure (2.27). The figure shows $GAL7$

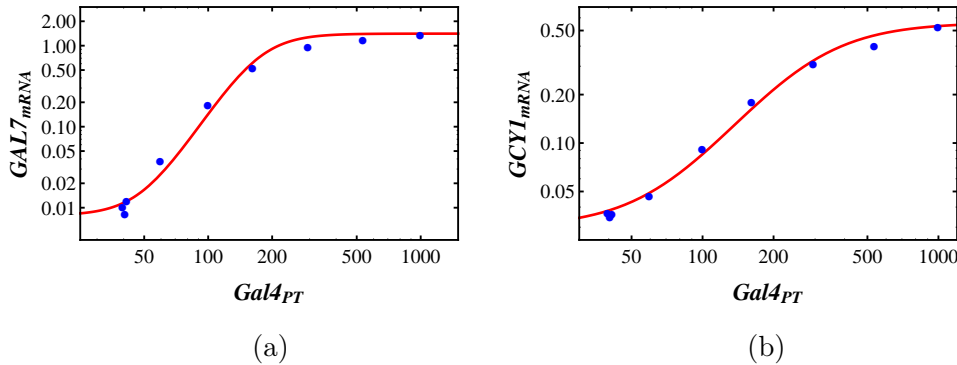


Figure 2.27: The results of nonlinear regression for (a) $GAL7$ mRNA and (b) $GCY1$ mRNA response to varying total Gal4p concentration in galactose using equation (2.48). The nonlinear data fit suggests that the response is very steep and a high level of cooperativity is needed.

and $GCY1$ promoter responses to the changing Gal4p protein. The parameter estimates and the corresponding standard errors and confidence intervals are given in Tables (2.4) and (2.5).

| Parameter | Estimate | Standard Error | Confidence Interval |
|-----------|----------|----------------|---------------------|
| n | 4.09 | 0.38 | (3.18, 5.001) |
| K_d | 172.68 | 14.74 | (137.81, 207.56) |

Table 2.4: Parameter estimates and the corresponding standard errors and confidence intervals for equation (2.48) and $GAL7$ mRNA data in Table (2.3).

| Parameter | Estimate | Standard Error | Confidence Interval |
|-----------|----------|----------------|---------------------|
| n | 2.2 | 0.12 | (1.91, 2.49) |
| K_d | 265.73 | 15.68 | (228.64, 302.82) |

Table 2.5: Parameter estimates and the corresponding standard errors and confidence intervals for equation (2.48) and *GCY1* mRNA data in Table (2.3).

The high Hill number suggest that both *GAL7* and *GCY1* mRNA responses are highly ultrasensitive. In fact, in both cases, the Hill numbers are unrealistically high. Strictly speaking, these numbers are bigger than the number of binding sites for each promoter which is theoretically impossible since the number of binding sites defines a limit for the highest possible Hill number. This already suggests that the Hill function alone is not sufficient to model the ultrasensitivity of the promoter response and therefore other sources of nonlinearity must be taken into account. We previously discussed that there are other well-know kinetic processes like molecular homodimerization and titration that can create ultrasensitivity in biological systems. In the first layer, Gal4p is the only protein of the system and therefore we can consider Gal4p homodimerization as another potential source of ultrasensitivity. In what follows, we will study the role of this mechanism and investigate how it can help reduce the high Hill number.

Homodimerization of Gal4p

In order to cope with the issue of very high Hill number (bigger than 2 for *GAL7* and bigger than 1 for *GCY1* mRNA responses), we take into account the homodimerization process as a well-known source of nonlinearity which can explain the high ultrasensitivity in the promoter response. At the presence of homodimerization, the Gal4p monomer protein binds another Gal4p protein to form an active dimer that can bind the promoter and induce transcription of *GAL7* and *GCY1* mRNA. The set of equations for this system reads as follows

$$\begin{aligned}
 \frac{d}{dt}Gal4_{PF} &= b_{G4} - 2k_{on4}Gal4_{PF}^2 + 2k_{off4}C4 - \gamma_{G4}Gal4_{PF}, \\
 \frac{d}{dt}C4 &= k_{on4}Gal4_{PF}^2 - k_{off4}C4 - \gamma_{G4}C4, \\
 \frac{d}{dt}M &= b_M + v_M \frac{C4^n}{K_d^n + C4^n} - \gamma_M M.
 \end{aligned}
 \tag{2.50}$$

In the above equations, $Gal4_{PF}$ is the Gal4p monomer and $C4$ is the Gal4p-Gal4p dimer protein. It is assumed that the monomer and dimer proteins have

the same decay rate constants. Since only the total concentration of Gal4p protein is available in the experimental data and we have no estimation of the free concentration, we need to convert the free concentration to the total one as we are constructing the mRNA response as a function of protein level. For this, we consider the following simple algebraic constraint

$$Gal4_{PF} + 2C4 = Gal4_{PT}, \quad (2.51)$$

which defines the mathematical relation between the total and free protein concentrations. Equations (2.50) are solved at the steady state together with equation (2.51) to give the mRNA M as a function of the total Gal4p concentration; that is,

$$M = B + V \frac{C4^n}{K_d^n + C4^n}, \quad (2.52)$$

with

$$C4 = \frac{1}{16}(\sqrt{\kappa_4} - \sqrt{8Gal4_{PT} + \kappa_4})^2, \quad (2.53)$$

where κ_4 is the lumped parameter and is defined by the following equation

$$\kappa_4 = \frac{k_{off4} + \gamma_{G4}}{k_{on4}}. \quad (2.54)$$

The new parameter κ_4 can be taken as the equilibrium dissociation rate constant for Gal4p-Gal4p binding. Now we can perform the nonlinear regression to fit equation (2.52) to the data in Table (2.3). Just like the previous section, we fix the values of V and B based on the highest level and lowest level of mRNA in Table (2.3). The main challenge in fitting equation (2.52) is that the three parameters n , K_d and κ_4 are highly correlated and as a result, the nonlinear regression generates very high standard errors that cannot be reduced even by varying initial values for the parameters. One solution is of course to fix as many parameters as possible [59]. We already mentioned that V and B can be fixed. The other choice could be either K_d or κ_4 . We let n be free because the value of this parameter can help us have a better understanding of how the ultrasensitivity in the response function can be controlled by the homodimerization mechanism. We also keep κ_4 free since our ultimate goal in this section is to see whether this nonlinear process can lead to the reduction of the Hill number. In fact, the nonlinear regression can be performed for a range of K_d values, from low values which represent a very strong Gal4p-promoter binding to high values which can be associated to weak Gal4p-promoter binding. Based on the kinetics of the homodimerization process, it is straightforward to see that K_d and κ_4 are negatively correlated; this means that high K_d values (weak Gal4p-promoter

binding) are compensated by low κ_4 values (strong homodimerization effect), and vice versa. We choose a value for K_d in order to make homodimerization compensate for high Hill number. Figure (2.28) shows that for $K_d = 0.5$, a very weak homodimerization can very well reduce the Hill number. The parameter

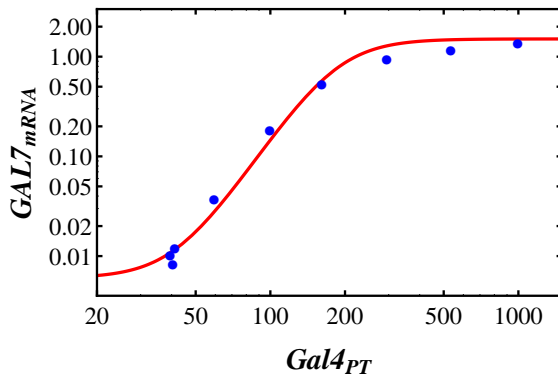


Figure 2.28: The result of nonlinear regression for $GAL7$ mRNA to varying total Gal4p concentration in galactose using equation (2.52) for $B = 0.008$, $V = 1.4$ and $K_d = 0.5$.

estimates and the corresponding standard errors and confidence intervals are given in Table (2.6). Figure (2.28) shows that for a weak homodimerization effect, it is possible to reduce the Hill number.

| Parameter | Estimate | Standard Error | Confidence Interval |
|------------|----------|----------------|---------------------|
| n | 1.86 | 0.14 | (1.51, 2.21) |
| κ_4 | 67199.8 | 11662.6 | (39622.3, 94777.5) |

Table 2.6: Parameter estimates and the corresponding standard errors and confidence intervals for equation (2.52) and $GAL7$ mRNA data in Table (2.3). The rest of parameters are fixed at $B = 0.008$, $V = 1.4$ and $K_d = 0.5$.

We can also check whether the homodimerization dissociation rate κ_4 in Table (2.6) reduces the Hill number for the $GAL7$ mRNA response. For this, we fix the value of κ_4 from Table (2.6) and perform the nonlinear regression for equation (2.52) with free K_d and n . The result of nonlinear regression is shown in Figure (2.29) and the parameter estimates are given in Table (2.7). It is clear that with the homodimerization strength reported in Table (2.6), the Hill number can be efficiently reduced to a value close to one.

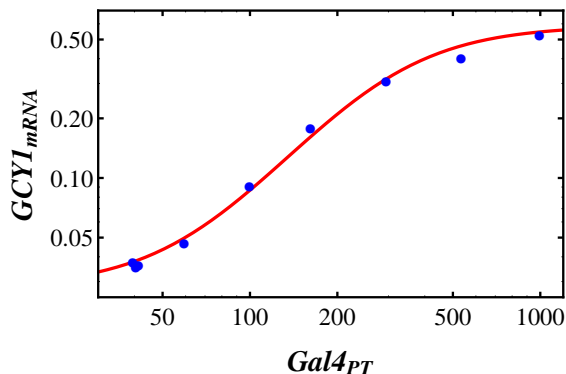


Figure 2.29: The result of nonlinear regression for $GCY1$ mRNA to varying total Gal4p concentration in galactose using equation (2.52) for $B = 0.028$, $V = 0.56$ and $\kappa_4 = 67200$.

| Parameter | Estimate | Standard Error | Confidence Interval |
|-----------|----------|----------------|---------------------|
| n | 1.02 | 0.05 | (0.9, 1.14) |
| K_d | 1.2 | 0.13 | (0.87, 1.52) |

Table 2.7: Parameter estimates and the corresponding standard errors and confidence intervals for equation (2.52) and $GCY1$ mRNA data in Table (2.3). The rest of parameters are fixed at $B = 0.028$, $V = 0.56$ and $\kappa_4 = 67200$.

Another mechanism that can be considered as a powerful nonlinear process is the titration or sequestration. This mechanism can generate strong ultrasensitive effects in the response of biological systems. We already know that in the first layer of the GAL network there is no Gal80p to sequester Gal4p proteins. However, we know that there are other promoters in the GAL network which are the target of Gal4p as the only transcription factor of the network. We argue that these promoters can act as titrants and sequester Gal4p proteins. We extend our model by including the explained titration mechanism. It should be noted that the strength of titration effect very much depends on the number of titrants, which are binding sites on the promoters, and the affinity of Gal4p proteins to them. Since we know that the number of these binding sites are not very high, we still keep the homodimerization to ultimately provide sufficient amount of nonlinearity.

Titration of Gal4p by extra binding sites

We extend our model to include the titration process of Gal4p proteins by extra binding sites. Since the homodimerization mechanism is also involved, we

assume that only Gal4p dimer proteins are sequestered. The set of equations for this system reads as follows

$$\begin{aligned}
 \frac{d}{dt}D_U &= -k_{on}^{tit}D_UC4 + k_{off}^{tit}D_B, \\
 \frac{d}{dt}D_B &= k_{on}^{tit}D_UC4 - k_{off}^{tit}D_B, \\
 \frac{d}{dt}Gal4_{PF} &= b_{G4} - 2k_{on4}Gal4_{PF}^2 + 2k_{off4}C4 - \gamma_{G4}Gal4_{PF}, \\
 \frac{d}{dt}C4 &= k_{on4}Gal4_{PF}^2 - k_{off4}C4 - k_{on}^{tit}D_UC4 + k_{off}^{tit}D_B - \gamma_{G4}C4, \\
 \frac{d}{dt}M &= b_M + v_M \frac{C4^n}{K_d^n + C4^n} - \gamma_M M.
 \end{aligned} \tag{2.55}$$

In the first two equations of (2.55), D_U and D_B represent the unbound and bound binding sites, respectively. The two parameters k_{on}^{tit} and k_{off}^{tit} also denote the association and dissociation rate constants of $C4$ -promoter binding for the extra binding sites. Since we do not have the number of free and bound sites, we add the following conservation equation for binding sites to the above dynamical equations

$$D_B + D_U = D_T, \tag{2.56}$$

with D_T as the total number of extra binding sites. Equation (2.51) will also become

$$Gal4_{PF} + 2C4 + 2D_B = Gal4_{PT}. \tag{2.57}$$

System (2.55) is solved at the steady state together with the two above algebraic constraints to get

$$M = B + V \frac{C4^n}{K_d^n + C4^n}, \tag{2.58}$$

with

$$C4 = F(Gal4_{PT}, b_{G4}, \kappa_4, \kappa^{tit}, D_T), \tag{2.59}$$

where κ_4 is defined by equation (2.54) and

$$\kappa^{tit} = \frac{k_{off}}{k_{on}}. \tag{2.60}$$

For simplicity, we put $\kappa^{tit} = K_d$, assuming that the affinity of Gal4p dimer to the main promoters is the same as the affinity to extra binding sites. Similar to the case of homodimerization, we have the problem of highly correlated parameters which makes the nonlinear regression fail to generate parameter estimates with reasonable standard errors. Therefore, like the previous cases, we try to fix as many parameters as possible. Since our goal is to see the effect of titration

on the ultrasensitivity and because the equilibrium dissociation constants are highly correlated with each other and n itself, we fix the value of κ_4 and K_d at $\kappa = 450$ and $K_d = 30$. Compared to Table (2.6), these values represent a much stronger homodimerization and a weaker Gal4p-promoter binding. It is reported in [71] that the number of extra binding sites are 15; therefore, we put $D_T = 15$. The result of nonlinear regression for *GAL7* mRNA data is depicted in Figure (2.30). The estimate value for n and the corresponding standard

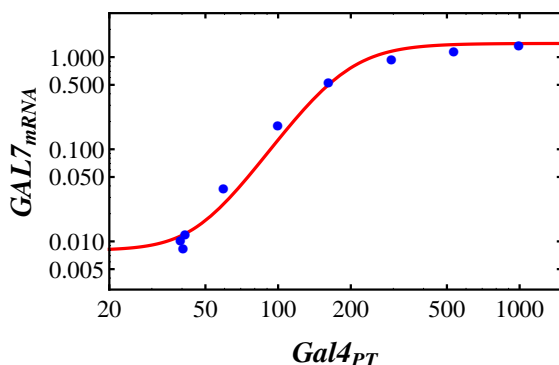


Figure 2.30: The result of nonlinear regression for *GAL7* mRNA response to varying total Gal4p concentration in galactose using equation (2.58). The value of the Hill number is $n = 1.83$ which shows that the titration together with homodimerization can create sufficient nonlinearity to explain the ultrasensitivity in the data.

error and confidence interval are given in Table (2.8).

| Parameter | Estimate | Standard Error | Confidence Interval |
|-----------|----------|----------------|---------------------|
| n | 1.83 | 0.1071 | (1.58415, 2.07806) |

Table 2.8: The estimate value of n and the corresponding standard error and confidence intervals for equation (2.58) and the *GAL7* mRNA data in Table (2.3). The rest of parameters are fixed: $B = 0.008$, $V = 1.4$, $K_d = 30$, $D_T = 15$ and $\kappa_4 = 450$.

The value of n in *GAL7* mRNA response is reasonably low. This confirms that the titration together with homodimerization can bring about enough nonlinearity to the model to explain the high ultrasensitivity in the Gal4p-mRNA data.

Summary and conclusions on the first layer

In the first layer of the *GAL* network, since *GAL80* is deleted, Gal4p which

is the transcription factor can freely induce the transcription of the mRNA of other genes. Therefore, at this very first layer, we can study the decay process of the protein and its interaction with the existing promoters. Our decay study on Gal4p protein confirms a half-life of 1.61 hours for this protein.

In the first step of Gal4p-promoter binding investigation, we used a simple Hill function. Our studies showed that the nonlinearity present in the mRNA level must be more complicated and the Hill function would not be enough to explain the high ultrasensitivity in the response. We fitted a simple Hill function to the mRNA data for *GAL7* and *GCY1* and observed that the Hill number is too high. In particular, the numbers are far bigger than the number of binding sites on the promoter of these two genes. In the second step of our analysis, we incorporated the homodimerization for the Gal4p protein which is a well-known mechanism in biochemical systems including the *GAL* network. Our investigations showed that a very weak homodimerization is able to dramatically reduce the Hill number. We also studied the role of titration mechanism through which the Gal4p dimer proteins are sequestered by extra binding sites; that is, the binding sites on the genes' promoters other than *GAL7* and *GCY1*. Our results showed that the titration mechanism together with a relatively strong homodimerization can also reduce the Hill number efficiently.

Next, we study the second layer of the *GAL* network and extend our existing model with Gal4p homodimerization to a bigger model that includes Gal80p interactions. We fix the parameter values for the Gal4p-Gal4p and Gal4p-promoter binding from the first layer and estimate the value of the new parameters for the extended model.

2.3.2 The 2nd layer of the galactose network: Gal80p decay data

In the second layer of the *GAL* network, the activity of Gal80p to repress Gal4p is isolated by deleting the *GAL3* and *GAL1* genes. In the absence of Gal3p and Gal1p proteins, Gal80p can freely bind Gal4p and repress the transcription of genes. It is worth noting that in the wild type cells, both Gal3p and Gal1p can bind Gal80p dimer proteins and release the repression of Gal4p by repressing Gal80p. The activity of both Gal3p and Gal1p constitute two important positive feedback loops of the *GAL* network [93]. In this layer, we will be able to study the decay process of Gal80p as well as Gal4p-Gal80p binding. We in particular investigate the two mechanisms of Gal80p homodimerization, and the titration of Gal4p by Gal80p proteins. In order to control variations

in the level of Gal80p, the endogenous promoter of *GAL80* has been replaced with a doxycycline repressible system. After the full activation of the system, the production of *GAL80* mRNA will be stopped and it can only be produced at the basal level.

2.3.2.1 Gal80p protein decay process in galactose

Table (2.9) shows the experimental data for the Gal80p decay process which present the reduction in the total concentration of Gal80p protein over time. The total concentration of Gal4p is also provided in the table. The concentration of Gal4p is assumed to be constant since this protein is constantly produced. Based on this assumption, we take the average of the values in the table and put $Gal4_{PT} = 535.13$. The data in Table (2.9) is obtained after shutting off the *GAL80* mRNA production at time zero.

| Time (h) | $Gal4_{PT}$ in galactose (N) | $Gal80_{PT}$ in galactose (N) |
|----------|------------------------------|-------------------------------|
| 0 | 497.45 | 1103.43 |
| 1.5 | 519.06 | 683.23 |
| 3 | 522.62 | 402.12 |
| 4.5 | 489.95 | 253.97 |
| 6 | 489.36 | 142.84 |
| 7.5 | 462.98 | 80.28 |
| 9 | 525.91 | 50.64 |
| 10.5 | 596.68 | 59.91 |
| 12 | 712.22 | 51.71 |

Table 2.9: Total concentration of Gal80p protein in galactose medium for different time points.

To study the decay process of Gal80p, we again perform the nonlinear regression to fit equation (2.43) ($Gal4_{PT}$ is replaced with $Gal80_{PT}$) to the data in Table (2.9). The Result of nonlinear regression is illustrated in Figure (2.31). The parameter estimates with the corresponding standard errors and confidence intervals are given in Table (2.10). According to the table and equation (2.43), the decay rate constant will be

$$\gamma_{G80} = 0.35 h^{-1}, \quad (2.61)$$

which is equivalent to the half-life of almost 2 hours. This already suggests that half-life of Gal80p protein is longer than Gal4p half-life.

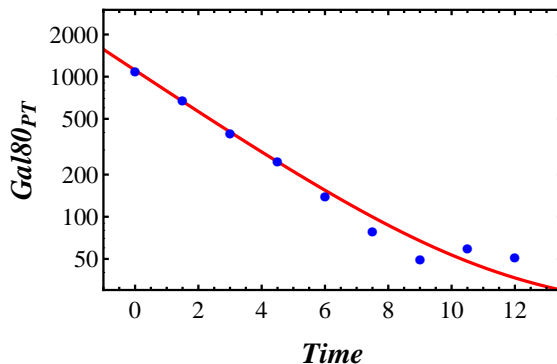


Figure 2.31: The result of nonlinear regression for total concentration of Gal80p protein in galactose medium using equation (2.43). The nonlinear data fit predicts that Gal80p has a half-life of almost 2 hours.

| Parameter | Estimate | Standard Error | Confidence Interval |
|-----------|----------|----------------|---------------------|
| Y | 30.62 | 12.34 | (-0.21, 60.21) |
| A | 1083.69 | 18.9 | (1037.44, 1129.94) |
| R | 0.35 | 0.01 | (0.32, 0.4) |

Table 2.10: Parameter estimates and the corresponding standard errors and confidence intervals for Gal80p decay data (2.9).

The basal expression rate is also given as

$$b_{G80} = 10.7 \text{ Nh}^{-1}. \quad (2.62)$$

Next, we will investigate the interaction of Gal80p proteins with Gal4p dimer proteins. We in particular calculate the parameter values for Gal80p homodimerization and Gal4p-Gal80p binding by investigating the effect of these mechanisms on the *GAL7* and *GCY1* mRNA response.

2.3.2.2 The regulatory effect of Gal80p protein on the *GAL7/GCY1* promoter response

In the absence of Gal3p and Gal1p proteins which act as inhibitors of Gal80p activity, Gal80p can freely bind Gal4p dimer proteins and repress the transcription of genes whose promoters are regulated by Gal4p proteins. Just like the previous sections, we study the response of *GAL7* and *GCY1* promoters. We already know from the first layer that homodimerization of Gal4p is essential in our mathematical model. We incorporate Gal80p homodimerization as well and take into account the sequestration of Gal4p dimer proteins by Gal80p

dimer proteins. Table (2.11) gives the total concentration of Gal80p and the corresponding *GAL7* and *GCY1* mRNA levels in galactose medium.

| <i>Gal80_{PT}</i> (N) | <i>GAL7</i> mRNA (N) | <i>GCY1</i> mRNA (N) |
|-------------------------------|----------------------|----------------------|
| 1103.43 | 0.002 | 0.017 |
| 683.23 | 0.003 | 0.017 |
| 402.12 | 0.006 | 0.02 |
| 253.97 | 0.02 | 0.044 |
| 142.84 | 0.12 | 0.089 |
| 80.28 | 0.53 | 0.19 |
| 50.64 | 1.26 | 0.29 |
| 59.91 | 1.64 | 0.45 |
| 51.71 | 2.69 | 0.71 |

Table 2.11: Total concentration of Gal80p protein in galactose medium with the corresponding *GAL7*/*GCY1* mRNA levels.

The data in Table (2.11) show that as the Gal80p decays, the production of mRNA increases since Gal4p proteins will be able to activate the promoters. Again, the above table can facilitate the study of both Gal80p decay and Gal80p-Gal4p binding processes with just one round of experimental measurement. The complete mathematical model for the nonlinear regression consists of three parts; the homodimerization of Gal4p and Gal80p proteins, the titration of Gal4p proteins by Gal80p proteins and finally the mRNA equation

$$\begin{aligned}
\frac{d}{dt}Gal4_{PF} &= -2k_{on4}Gal4_{PF}^2 + 2k_{off4}C4, \\
\frac{d}{dt}C4 &= k_{on4}Gal4_{PF}^2 - k_{off4}C4 - k_{on480}C4C80 + k_{off480}C480 - \gamma_{G4}C4, \\
\frac{d}{dt}Gal80_{PF} &= b_{G80} - 2k_{on80}Gal80_{PF}^2 + 2k_{off80}C80 - \gamma_{G80}Gal80_{PF}, \\
\frac{d}{dt}C80 &= k_{on80}Gal80_{PF}^2 - k_{off80}C80 - k_{on480}C4C80 + k_{off480}C480 - \gamma_{G80}C80, \\
\frac{d}{dt}C480 &= k_{on480}C4C80 - k_{off480}C480, \\
\frac{d}{dt}M &= b_M + v_M \frac{C4^n}{K_d^n + C4^n + C480^n} - \gamma_M M,
\end{aligned}
\tag{2.63}$$

with *C80* as the Gal80p dimer protein and *C480* as the complex of *C4* and *C80*. We do not consider any basal production or decay rate for Gal4p since it is constitutively produced. We also assume that the Gal4p-Gal80p complex

does not decay. The following equations are taken into account for the total concentration of Gal4p and Gal80p proteins

$$\begin{aligned} Gal4_{PF} + 2C4 + 2C480 &= Gal4_{PT}, \\ Gal80_{PF} + 2C80 + 2C480 &= Gal80_{PT}, \end{aligned} \quad (2.64)$$

where $Gal4_{PT}$ and $Gal80_{PT}$ are the total concentrations of Gal4p and Gal80p proteins. System (2.63) is solved at the steady state together with the two above algebraic constraints to get

$$M = B + V \frac{C4^n}{K_d^n + C4^n + C480^n}, \quad (2.65)$$

with

$$\begin{aligned} C4 &= F(Gal4_{PT}, Gal80_{PT}, \kappa_4, \kappa_{80}, \kappa_{480}), \\ C80 &= G(Gal4_{PT}, Gal80_{PT}, \kappa_4, \kappa_{80}, \kappa_{480}), \end{aligned} \quad (2.66)$$

where

$$\kappa_4 = \frac{k_{off4} + \gamma_4}{k_{on4}}, \quad \kappa_{80} = \frac{k_{off80} + \gamma_{80}}{k_{on80}}, \quad \kappa_{480} = \frac{k_{off480}}{k_{on480}}. \quad (2.67)$$

Using the parameter values from the first layer, we put $n = 1.83$, $K_d = 0.5$, $\kappa_4 = 67200$. We also fix $\kappa_{80} = 700$ based on the in vitro data from [54] that reports a hundred-time difference between κ_4 and κ_{80} values. We perform the nonlinear regression to fit equation (2.65) to the *GAL7* mRNA data. The result of nonlinear regression is depicted in Figure (2.32). The nonlinear regression

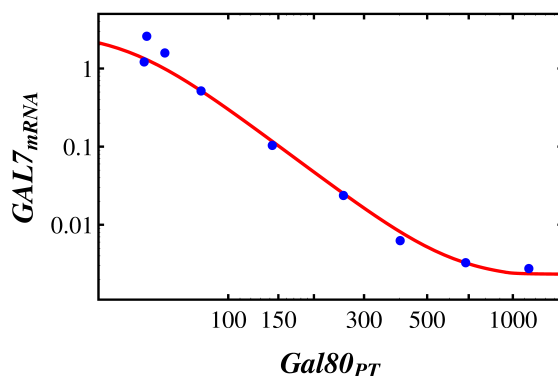


Figure 2.32: The result of nonlinear regression for *GAL7* mRNA response to varying total Gal80p concentration in galactose using equation (2.65) for parameter values $B = 0.002$, $V = 3$, $K_d = 0.5$, $\kappa_4 = 67200$, $\kappa_{80} = 700$, and $n = 1.83$. The nonlinear regression yields $\kappa_{480} = 1.62$ which represents a very strong titration effect.

yields $\kappa_{480} = 1.62$ which corresponds to a strong titration effect. We use this value and fix other parameters (except the Hill number) to fit equation (2.65) to the *GCY1* mRNA data in order to check whether this strong titration can explain the ultrasensitivity in the *GCY1* mRNA response. The result of nonlinear regression is shown in Figure (2.33). The nonlinear regression yields

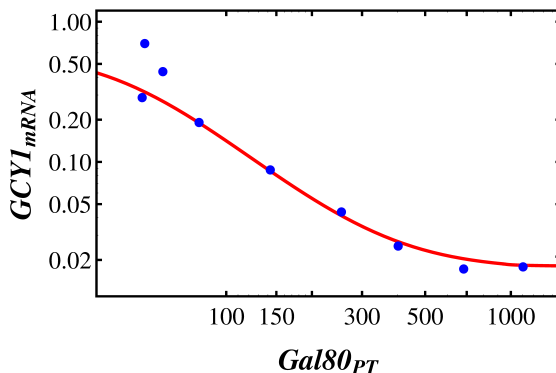


Figure 2.33: The result of nonlinear regression for *GCY1* mRNA response to varying total Gal80p concentration in galactose using equation (2.65) for parameter values $B = 0.015$, $V = 0.7$, $K_d = 1.2$, $\kappa_4 = 67200$, $\kappa_{80} = 700$ and $\kappa_{480} = 1.62$. The nonlinear regression yields $n = 1.05$ which shows that a strong titration and a weak homodimerization can create sufficient nonlinearity to explain the ultrasensitivity in the mRNA response.

$n = 1.05$. Our analyses in the second layer show how the homodimerization and titration mechanisms can describe the ultrasensitivity in the *GAL7* and *GCY1* mRNA response. The nonlinear regression yields high standard errors in both cases above which is mainly because of the complexity of equations.

Summary and conclusions on the second layer

In the second layer of the *GAL* network, since *GAL1* and *GAL3* are deleted, Gal80p can freely represses the activity of transcription factor Gal4p by sequestering this protein into an inactive complex on the promoter. Therefore, the experimental data in this layer enables us to isolate the interaction of Gal80p with Gal4p. Our decay study on Gal80p protein also confirms a half-life of almost 2 hours for this protein which is longer than that of Gal4p.

In our mathematical investigation of the second layer, we incorporated homodimerization mechanism for both Gal4p and Gal80p proteins and in addition to that considered the titration of Gal4p dimer proteins by Gal80p dimer proteins.

Because of the complexity of algebraic equations and the high correlation between many parameters in our model, we fixed as many parameters as possible by using values from the first layer and reported in vitro parameter values in the literature. As we get to the higher layers of the *GAL* network, the complexity of the model grows, and using the nonlinear regression becomes more difficult.

Next, we study the third layer by extending our model to a yet bigger model by including Gal1p protein interactions. Our goal in this layer is to reconstruct bistability by using the input-output response of the network that is obtained by opening the *GAL1* positive feedback loop.

2.3.3 The third layer of the galactose network: Opening the *GAL1* feedback loop

In the third layer of the *GAL* network, the negative feedback by the Gal8p protein remains intact and in addition to this protein and Gal4p, *GAL1* mRNA and its protein Gal1p are also taken into account. At the presence of galactose, the Gal80p protein is sequestered by Gal1p so that the repression of Gal4p by Gal80p protein will be released. Since Gal4p protein binds the *GAL1* promoter to induce the transcription of the gene, Gal1p activity constitutes a positive feedback loop. In this layer, the *GAL* network is opened from the *GAL1* feedback loop to reconstruct the bistable behavior of the network by using the input-output response. Experimentally, the *GAL1* feedback loop is opened by replacing the endogenous promoter of *GAL1* with a doxycycline repressible system to control the input, and for the output, the *YFP* mRNA level is controlled by the *GAL1* endogenous promoter.

For Gal4p protein and its dimer *C4*, the corresponding equations in (2.63) are used. For Gal80p and its dimer, the previous equations need to be updated since this protein interacts with Gal1p protein. The updated version of Gal80p and the dimer *C80* equations are given as follows

$$\begin{aligned}
 \frac{d}{dt}Gal80_{PF} &= \\
 b_{G80} + v_{80} \frac{C4}{K_{d80} + C4 + C480} - 2k_{on80}Gal80_{PF}^2 + 2k_{off80}C80 - \gamma_{G80}Gal80_{PF}, \\
 \frac{d}{dt}C80 &= k_{on80}Gal80_{PF}^2 - k_{off80}C80 - k_{on480}C4C80 + k_{off480}C480 - \gamma_{G80}C80 \\
 &\quad - k_{on180}Gal1_{Act}^2C80 + k_{off180}C180,
 \end{aligned}
 \tag{2.68}$$

where for simplicity, the Hill number is fixed at one since the *GAL80* promoter has only one binding site. In fact, the presence of Hill function in the first equation above implies the *GAL80* negative feedback loop. Gal80p dimer proteins are sequestered by the active form of Gal1p proteins, represented by *Gal1_{Act}* in the above equations. The Gal1p gets activated by binding to the galactose, and the activated form of this protein will bind Gal80p to release its repression of Gal4p. The full set of equations for *GAL1* mRNA and Gal1p protein are given by

$$\begin{aligned}
 \frac{d}{dt}GAL1_M &= b_{G1} + v_1 \frac{C4^n}{K_{d1}^n + C4^n + C480^n} - \gamma_M GAL1_M, \\
 \frac{d}{dt}Gal1_{PF} &= \mu Gal1_M - k_{on1}GalGal1_{PF} + k_{off1}Gal1_{Act} - \gamma_{G1}Gal1_{PF}, \\
 \frac{d}{dt}Gal1_{Act} &= k_{on1}GalGal1_{PF} - k_{off1}Gal1_{Act} - 2k_{on180}Gal1_{Act}^2 C80 \\
 &\quad + 2k_{off180}C180 - \gamma_{G1}Gal1_{Act} \\
 \frac{d}{dt}C180 &= k_{on180}Gal1_{Act}^2 C80 - k_{off180}C180,
 \end{aligned} \tag{2.69}$$

where *Gal1_{PF}* is the free Gal1p protein and *C180* is the complex of active Gal1p with the Gal80p dimer protein. We assume that the complex proteins do not decay. Finally, the following simple binding equation represents the galactose dynamics

$$\frac{d}{dt}Gal = -k_{on1}GalGal1_{PF} + k_{off1}Gal1_{Act}. \tag{2.70}$$

For the conversion of the free concentrations into the total ones, we also consider the following algebraic constraints

$$\begin{aligned}
 Gal4_{PF} + 2C4 + 2C480 &= Gal4_{PT}, \\
 Gal80_{PF} + 2C80 + 2C480 + 2C180 &= Gal80_{PT}, \\
 Gal + Gal1_{Act} + 2C180 &= Gal_T,
 \end{aligned} \tag{2.71}$$

with *Gal_T* as the total concentration of galactose. In an input-output setting where the *GAL1* feedback loop is opened at the mRNA level, *GAL1_M* is replaced with the constant ω as the input in the second equation of (2.69), and the rest of *GAL1_M* variables are treated as the output. In order to find the input-output function, the dynamical equations should be solved at the steady state together with equations (2.71) to express *GAL1_M* as a function of ω . Because of the complexity of equations, it is impossible to solve for all intermediate variables and get a single equation for the input-output function. Instead, we keep the free

concentration of Gal80p ($Gal80_{PF}$) and express $GAL1_M$ and ω as parametrized functions of this variable. Since we cannot perform the nonlinear regression for the explained complicated input-output relation, we fix all the parameters from the previous layers and use the reported in vitro parameter values in the literature to build the input-output response of the function. We fix $n = 2$ for the $GAL1$ promoter since its behavior is very similar to the $GAL7$ promoter. For the $GAL80$ promoter, we take $b_{G80} = 30$, $v_{80} = 180$ and $K_{d80} = 1$ and for the $GAL1$ promoter, we take $b_{G1} = 0.002$, $v_1 = 5$ and $K_{d1} = 0.5$ (the same as the Gal4p- $GAL7$ promoter binding). The decay rate of $GAL1$ mRNA is fixed at $\gamma_{G1} = 5.13$ which is equivalent to the half life of 8 min [35]. For simplicity, all protein decay rates are fixed at the value of 0.35. For the equilibrium dissociation constant of Gal1p-Gal80p binding and Gal1-galactose binding we put

$$\kappa_{180} = \frac{k_{off180}}{k_{on180}} = 10 \quad \text{and} \quad \kappa_1 = \frac{k_{off1}}{k_{on1}} = 4 \times 10^7, \quad (2.72)$$

based on the reported in vitro data in [14]. The rest of parameters are fixed from the previous layers. Using the parameter values mentioned above, the input-output response of the network can be constructed and is shown in Figure (2.34) for different galactose total concentrations. The response diagram

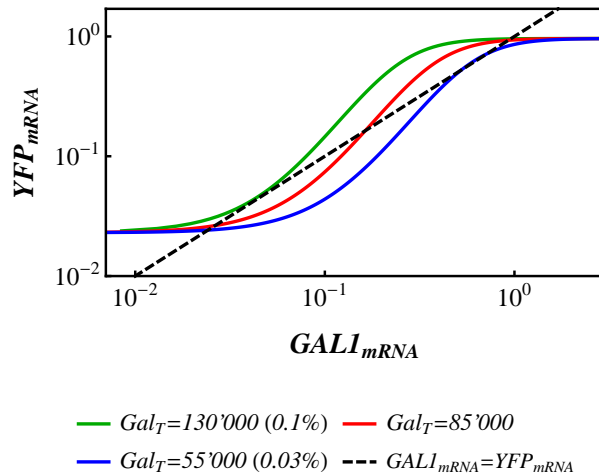


Figure 2.34: The graph of input-output response of the GAL network in the third layer. The response is achieved by opening the $GAL1$ positive feedback loop. The bistability range is detected between 0.03% and 0.1% galactose.

clearly shows the existence of bistability for a range of 0.03% to 0.1% galactose. This bistability range is narrow compared to the experimentally measured bistability range [1]. One potential reason might be because of the level of ul-

trasensitivity in the model which does not give a broad bistability range. Extra source of nonlinearity for a more ultrasensitive response can be created for example by assuming that the Gal1p protein can sequester Gal80p dimer proteins even without galactose [69]. However, we should also consider the level of complexity that detailed molecular interactions can add to the model.

Summary and conclusions on the third layer

In the third layer of the *GAL* network, the three proteins Gal4p, Gal80p and Gal1p interact with each other to create bistability. The activity of Gal80p constitutes a negative feedback loop while Gal1p protein encloses a positive feedback loop. Gal1p can release the repression of transcription factor Gal4p by binding Gal80p proteins. We developed a mathematical model that includes the two feedback loops and the interactions of the three proteins. We opened the *GAL1* feedback loop at the mRNA level and constructed the input-output response with which we could show the bistability for a range of galactose concentrations.

Chapter 3

Conclusions

Bistability, the ability of a dynamical system to create two distinct stable steady states, is the corner stone of many decision-making processes in biological systems. The importance of bistability have been long recognized in prokaryotic organisms like the *lac* operon in *Escherichia coli* as well as the eukaryotic organisms like the galactose metabolic network in *Saccharomyces cerevisiae*. The two main ingredients of bistability in biological and biochemical networks are the positive feedback loops and ultrasensitivity. Positive feedback loops are ubiquitous biological motifs whose presence is the necessary condition for bistability. Ultrasensitivity can emerge as a result of different nonlinear mechanisms like molecular cooperativity, homodimerization and molecular titration in gene regulatory networks. Examples of these mechanisms can be found in particular in biological systems which are capable of demonstrating bistability and memory like the galactose network. A very vital requirement for many such systems is to maintain the bistable behavior under the perturbations in the environment. This raises the issue of robustness in biological systems which is defined as the ability of a system to resist variations in its parameter values.

In this thesis, we addressed the issue of robustness from two different points of view. First, we studied conditions on the parameter configurations in a bistable system to maximize the bistability range of a single parameter. Second, we focused on the unstable steady state as a key player in creating and maintaining bistability and explored regions inside the bistability area in which the unstable steady state has the minimum sensitivity to parameter perturbations. All formulations for the study of bistability robustness were carried out by employing the open-loop approach and in particular the open-loop sensitivity. The open-loop approach was also utilized to study bistability in the *GAL* network by reconstructing the input-output response of the network that was obtained

by opening the network from the *GAL1* positive feedback loop.

3.1 Extrema in the bistability range of a single parameter

Bistability range of parameters determines how much a parameter can be varied without losing the bistable behavior. In a two-dimensional parameter space, the boundaries of bistability region are given by the bifurcation curves like the saddle-node bifurcation. The intersection of these curves happen at the bifurcation points of higher codimensions like the cusp point. These points already define the extremum of the bistability range for the parameters in a two-dimensional parameter space. The position of a cusp point can be varied by changing a third parameter; as a result of this variation, the bistability range of a single parameter can be increased. This means that there is a possibility to maximize this range for a single parameter. This is of high importance since enlarging a parameter's bistability range can make the bistability robust with regard to variations of that specific parameter. Moreover, this allows the system to capture a wider region in the parameter space which may include physically realizable parameter values. In the first section of chapter 2, we discussed how we can address the problem of finding extrema in the locus of cusp points in a system that consists of a self positive, and a negative feedback loop that operates under the molecular titration. Using this system in particular reveals that the negative feedback (at least in some specific architectures) can potentially contribute to the bistability by increasing the bistability range of a single parameter. This is a very interesting observation since the negative feedback loops are known to weaken the bistability in feedback systems. Another importance of this piece of study is the use of the open-loop system features like the open-loop sensitivity. We used the logarithmic sensitivity of the output to the input and found out that maximum of sensitivity curves vary nonmonotonically with some parameters. We observed that in specific cases, the maximum of maximum sensitivity with respect to the input and a parameter can be corresponded to the extremum of the locus of bifurcation points which ultimately gives the biggest bistability range for another parameter. It was shown that this might not be always the case and more parameters need to be included in the analysis. A detailed formulation of the parameter configurations that lead to the detection of the extrema has recently been done in [53]. According to this formulation, the extremum of the bistability range for a specific parameter can be detected if the open-loop sensitivity is maximized with respect to two other parameters. The formulation also provides information on how these two other parameters can be selected.

3.2 Robust regions in the bistability area

In the second section of the thesis, we focused on the study of bistability robustness in three simple mathematical models of gene networks which consist of a simple positive feedback loop and an ultrasensitive mechanism. We first analyzed a one-gene positive feedback loop with cooperativity mechanism and later modified the system by replacing cooperativity with homodimerization and molecular titration. We studied the existence of bistability in all these systems and as a measure of robustness turned our focus to the maintenance of the unstable steady state under parameter perturbations. Unstable steady states are key to the existence and maintenance of biological switches. We in particular established mathematical conditions under which the sensitivity of unstable steady state can be minimized with respect to parameters of a system. To this end, we used the open-loop approach and employed the open-loop sensitivity of the feedback system to derive mathematical conditions for the minimization of the unstable steady state sensitivity to parameters. We showed that minimization of the unstable steady state sensitivity to parameters will lead to the definition of new boundaries inside the bistability area. We defined the robust bistability region to be the most inner parameter region bounded by the sensitivity boundaries. We showed that the total sensitivity of the unstable steady state to all parameters takes its minimum inside the robust bistability region. Our results shed light on the role of different parameters and regulatory motifs like the homodimerization and molecular titration in creating robust bistability. Using the open-loop approach is a novel technique that helps us detect robust bistable regions in the parameter space without the need to struggle with the complexity of closed-loop system to construct the bifurcation diagrams which is a very difficult task in large dynamical systems. In fact, Angeli et al. [5] first used this technique to detect the existence of bistability by directly using the input-output response of the open-loop version of a monotone feedback system. Our approach can be used to study other system architectures like the double-positive and double negative feedback loops. These systems are two-gene positive feedback loop systems with the cooperativity mechanism and their bifurcation diagrams have a quite similar structure as the one-gene system with titration.

3.3 Bistability in the *GAL* network

The galactose metabolic network in *Saccharomyces cerevisiae* is a well-known model organism that provides a very rich framework to study molecular inter-

actions and feedback loops. The network has one negative feedback and several positive feedback loops and a number of regulatory and structural genes that help the network metabolize the galactose as a carbon source. We used the in vivo experimental data to study bistability in the *GAL* network by developing a mathematical model that expresses the input-output response of the network. We performed nonlinear regression to find the parameter values in our model using different layers of the network. The biggest challenge of performing the nonlinear regression for large models like the *GAL* network is the complexity of mathematical equations that model these networks. This problem can be tackled by isolating different parts of the network by introducing deletion strains. As a result of deleting genes, the interaction of proteins in different layers can be isolated and studied separately. We particularly studied three layers of the *GAL* network; in the first layer, *GAL80* gene is deleted and as a result, the activity of Gal4p protein is isolated since in the absence of Gal80p protein, Gal4p dimer proteins bind the promoter of the network genes and initiate their transcription. The Gal4p experimental data was used to study both the decay process and the interaction of this protein with promoters. We studied the effect of the total concentration of Gal4p on the level of *GAL7* and *GCY1* mRNA as the protein decays. Our studies revealed that a very weak homodimerization needs to be incorporated into the model to explain the ultrasensitivity in the mRNA response. We also investigated the role of another nonlinear mechanism which is the titration by extra binding sites (binding sites on the promoters other than *GAL7* and *GCY1*) and showed that for a strong homodimerization effect, titration can also very well describe the ultrasensitivity in the mRNA response. Our studies continued to the second layer by extending model to include Gal4p and Gal80p interaction. In the absence of *GAL1* and *GAL3* genes in the second layer, Gal80p dimer proteins can freely sequester Gal4p dimer proteins on the promoter into inactive complexes. In this layer, we studied the decay process of Gal80p and its interaction with Gal4p proteins. Our investigations approved that in the presence of Gal4p and Gal80p homodimerization and a very strong titration effect, the ultrasensitivity in the mRNA data can very well be modeled. The titration mechanism in this layer acts based on the sequestration of Gal4p dimer proteins by the Gal80p dimer proteins. We performed the nonlinear regression in the first two layers to estimate the parameter values of the model. The model itself became more complicated as the new molecular components were added in each layer. The main challenge of performing nonlinear regression in both layers is the presence of highly correlated parameters. The high correlation can generate large standard errors in the fitting process and reduce

the quality of the fit. One solution is to fix as many parameters as possible. We fixed the homodimerization parameter for Gal4p as well as the Gal4p-promoter binding parameters in the second layer, by using the values from the first layer. For the Gal80p-Gal80p binding, we used the in vitro data reported in the literature. We then estimated the Gal4p-Gal80p binding constant by fitting the *GAL7* mRNA data and further validated the result by fitting the model to the *GCY1* data. In the third layer, we added the dynamics of *GAL1* mRNA and protein to the system and extended our model to include the titration of Gal80p dimer proteins by Gal1p proteins. We opened the system from the *GAL1* mRNA level and solved the equations to obtain the input-output response function of the network. Because of the complexity of equations, it was impossible to get an explicit equation that gives the output as a function of the input. Therefore, we expressed the response of the network as a parametrized function of other variables and parameters. We used the in vitro values and the results of the first two layers to fix the parameter values. Our results successfully reconstructed the bistability for a range of galactose concentrations. Our bistability range was, however, narrower than that of reported in the literature. We argued that this can be because of the insufficient level of ultrasensitivity in our response function that can be compensated for example by assuming that the Gal1p protein can sequester Gal80p dimer proteins even without galactose. Adding more molecular mechanisms and interactions to the systems can potentially give a better understanding of the dynamics of biochemical systems, but at the same time it will add to the complexity of equations and the analysis of such systems. Our investigations revealed the significance of ultrasensitive regulatory motifs like homodimerization and titration in creating bistability in the *GAL* network.

Published articles related to the thesis:

I. Majer, **A. Hajhosseini** and A. Becskei.

Identification of optimal parameter combinations for the emergence of bistability.

Physical Biology 12 (2015) 066011.

Bibliography

- [1] M. Acar, A. Becskei, and A. van Oudenaarden. Enhancement of cellular memory by reducing stochastic transitions. *Nature*, 435:228–232, 2005. [5](#), [47](#), [67](#)
- [2] U. Alon. *An Introduction to Systems Biology: Design Principles of Biological Circuits*. Taylor & Francis Group, 2006. [1](#)
- [3] U. Alon, M. G. Surette, N. Barkai, and S. Leibler. Robustness in bacterial chemotaxis. *Nature*, 397:168–171, 1999. [7](#)
- [4] D. Angeli and E. D. Sontag. Monotone control systems. *IEEE Transactions on Automatic Control*, 48:1684–1698, 2003. [12](#)
- [5] D. Angeli, Jr. J. E. Ferrell, and E. D. Sontag. Detection of multistability, bifurcations, and hysteresis in a large class of biological positive-feedback systems. *Proceedings of the National Academy of Sciences of USA*, 101:1822–1827, 2004. [12](#), [71](#)
- [6] R. Apostu and M. C. Mackey. Mathematical model of gal regulon dynamics in *saccharomyces cerevisiae*. *Journal of Theoretical Biology*, 293:219–235, 2012. [5](#), [47](#)
- [7] M. R. Atkinson, M. A. Savageau, J. T. Myers, and A. J. Ninfa. Development of genetic circuitry exhibiting toggle switch or oscillatory behavior in *Escherichia coli*. *Cell*, 113:597–607, 2003. [5](#)
- [8] E. Z. Bagci, Y. Vodovotz, T. R. Billiar, G. B. Ermentrout, and I. Bahar. Bistability in apoptosis: roles of bax, bcl-2, and mitochondrial permeability transition pores. *Biophysical Journal*, 90:1546–1559, 2006. [5](#)
- [9] N. Barkai and S. Leibler. Robustness in simple biochemical networks. *Nature*, 387:913–917, 1997. [7](#)

- [10] A. Becskei. Linearization through distortion: a new facet of negative feedback in signaling. *Molecular Systems Biology*, 5:255, 2009. [17](#)
- [11] A. Becskei and L. Serrano. Engineering stability in gene networks by autoregulation. *Nature*, 405:590–593, 2000. [1](#), [17](#)
- [12] A. Becskei, B. Seraphin, and L. Serrano. Positive feedback in eukaryotic gene networks: cell differentiation by graded to binary response conversion. *The EMBO Journal*, 20:2528–2535, 2001. [1](#), [5](#)
- [13] P. J. Bhat. *Galactose regulon of yeast. From genetics to systems biology*. Springer, 2008. [5](#), [47](#)
- [14] P.J. Bhat and J. E. Hopper. Overproduction of the gal1 or gal3 protein causes galactose-independent activation of the gal4 protein: evidence for a new model of induction for the yeast gal/mel regulon. *Molecular Cell Biology*, 12:2701–2707, 1992. [67](#)
- [15] N. E. Buchler and F. R. Cross. Protein sequestration generates a flexible ultrasensitive response in a genetic network. *Molecular Systems Biology*, 5:272, 2009. [5](#), [42](#)
- [16] N. E. Buchler and M. Louis. Molecular titration and ultrasensitivity in regulatory networks. *Journal of Molecular Biology*, 384:1106–1119, 2008. [5](#), [36](#), [41](#)
- [17] B. Chen, Y. Wang, W. Wu, and W. Li. A new measure of the robustness of biochemical networks. *Bioinformatics*, 21:2698–2705, 2005. [8](#)
- [18] J. L. Cherry and F. R. Adler. How to make a biological switch. *Journal of Theoretical Biology*, 203:117–133, 2000. [5](#), [14](#)
- [19] C. Cosentino, L. Salerno, A. Passanti, A. Merola, D. G. Bates, and F. Amato. Structural bistability of the gal regulatory network and characterization of its domains of attraction. *Journal of Computational Biology*, 19:148–162, 2012. [47](#)
- [20] A. Dayarian and A. M. Sengupta. Titration and hysteresis in epigenetic chromatin silencing. *Physical Biology*, 10:036005, 2013. [5](#)
- [21] M. B. Elowitz and S. Leibler. A synthetic oscillatory network of transcriptional regulators. *Nature*, 403:335–338, 2000. [1](#), [17](#)

- [22] R. J. Field and R. M. Noyes. Oscillations in chemical systems: Iv. limit cycle behavior in a model of a real chemical reaction. *The Journal of Chemical Physics*, 60:1877–1884, 1974. [1](#)
- [23] R. J. Field, E. Koros, and R. M. Noyes. Oscillations in chemical systems: Ii. thorough analysis of temporal oscillation in the bromate–cerium–malonic acid system. *Journal of The American Chemical Society*, 94:8649–8664, 1972. [1](#)
- [24] S. E. Fraser and R. M. Harland. The molecular metamorphosis of experimental embryology. *Cell*, 100:41–55, 2000. [1](#)
- [25] T. S. Gardner, C. R. Cantor, and J. J. Collins. Construction of a genetic toggle switch in *Escherichia coli*. *Nature*, 403:339–342, 2000. [1](#), [5](#)
- [26] C. Gerard, J. J. Tyson, and B. Novak. Minimal models for cell-cycle control based on competitive inhibition and multisite phosphorylations of cdk substrates. *Biophysical Journal*, 104:1367–1379, 2013. [5](#)
- [27] A. Ghosh and B. Chance. Oscillations of glycolytic intermediates in yeast cells. *Biochemical and Biophysical Research Communications*, 16:174–181, 1964. [1](#)
- [28] E. Giniger and M. Ptashne. Cooperative dna binding of the yeast transcriptional activator *gal4*. *Proceedings of the National Academy of Sciences of USA*, 85:382–386, 1988. [47](#)
- [29] D. Gonze, J. Halloy, and A. Goldbeter. Robustness of circadian rhythms with respect to molecular noise. *Proceedings of the National Academy of Sciences of USA*, 99:673–678, 2002. [7](#)
- [30] J. S. Griffith. Mathematics of cellular control processes: Ii. positive feedback to one gene. *Journal of Theoretical Biology*, 20:209–216, 1968. [6](#)
- [31] J. Guckenheimer and P. Holmes. *Nonlinear Oscillations, Dynamical Systems and Bifurcations of Vector Fields*. Springer-Verlag, 1990. [2](#), [8](#)
- [32] L. H. Hartwell, J. J. Hopfield, S. Leibler, and A. W. Murray. From molecular to modular cell biology. *Nature*, 402:C47–C52, 1999. [1](#)
- [33] J. Hasty, D. McMillen, F. Isaacs, and J. J. Collins. Computational studies of gene regulatory networks: in numero molecular biology. *Nature Reviews Genetics*, 2:268–279, 2001. [1](#)

- [34] A. V. Hill. The possible effect of the aggregation of the molecules of haemoglobin on its dissociation curves. *Journal of Physiology*, 40:4–7, 1910. [2](#)
- [35] C. Hsu, S. Scherrer, A. Buetti-Dinh, P. Ratna, J. Pizzolato, V. Jaquet, and A. Becskei. Stochastic signalling rewires the interaction map of a multiple feedback network during yeast evolution. *Nature Communications*, 3:682, 2012. [67](#)
- [36] S. Huang, Y. Guob, G. Mayb, and T. Enverb. Bifurcation dynamics in lineage-commitment in bipotent progenitor cells. *Developmental Biology*, 305:695–713, 2007. [5](#)
- [37] B. Ingalls. Sensitivity analysis: from model parameters to system behaviour. *Essays in Biochemistry*, 45:177–193, 2008. [11](#)
- [38] F. J. Isaacs, J. Hasty, C. R. Cantor, and J. J. Collins. Prediction and measurement of an autoregulatory genetic module. *Proceedings of the National Academy of Sciences of USA*, 100:7714–7719, 2003. [5](#)
- [39] F. Jacob and J. Monod. Genetic regulatory mechanisms in the synthesis of proteins. *Journal of Molecular Biology*, 3:318–356, 1961. [1](#)
- [40] H. K. Khalil. *Nonlinear systems*. Prentice Hall, 1995. [3](#)
- [41] H. Kitano. Systems biology: a brief overview. *Science*, 295:1662–1664, 2002. [1](#)
- [42] H. Kitano. Biological robustness. *Nature Reviews Genetics*, 5:826–837, 2004. [8](#)
- [43] H. Kitano. Towards a theory of biological robustness. *Molecular Systems Biology*, 3:137, 2007. [8](#)
- [44] H. Kitano. Violations of robustness trade-offs. *Molecular Systems Biology*, 6:384, 2010. [8](#)
- [45] B. P. Kramer and M. Fussenegger. Hysteresis in a synthetic mammalian gene network. *Proceedings of the National Academy of Sciences of USA*, 102:9517–9522, 2005. [5](#)
- [46] Y. A. Kuznetsov. *Elements of Applied Bifurcation Theory*. Springer-Verlag, 1998. [8](#), [9](#), [10](#), [19](#)
- [47] S. Lang. *Fundamentals of Differential Geometry*. Springer, 1999. [31](#)

- [48] S. Legewie, N. Bluethgen, and H. Herzel. Mathematical modeling identifies inhibitors of apoptosis as mediators of positive feedback and bistability. *PLoS Computational Biology*, 2:e120, 2006. [5](#)
- [49] H. M. Lodhi, S. H. Muggleton, and J. Gunawardena. *Models in Systems Biology: The Parameter Problem and the Meanings of Robustness*. John Wiley & Sons, 2010. [8](#)
- [50] A. J. Lotka. *Elements of Physical Biology*. Williams and Wilkins Company, 1925. [1](#)
- [51] L. Ma and P. A. Iglesias. Quantifying robustness of biochemical network models. *BMC Bioinformatics*, 3:38, 2002. [8](#), [33](#)
- [52] Y. T. Maeda and M. Sano. Regulatory dynamics of synthetic gene networks with positive feedback. *Journal of Molecular Biology*, 359:1107–1124, 2006. [5](#)
- [53] I. Majer, A. Hajihosseini, and A. Becskei. Identification of optimal parameter combinations for the emergence of bistability. *Physical Biology*, 12:066011, 2015. [26](#), [70](#)
- [54] K. Melcher and H. E. Xu. Gal80-gal80 interaction on adjacent gal4p binding sites is required for complete gal gene repression. *EMBO Journal*, 20:841–851, 2001. [47](#), [63](#)
- [55] J. Monod. From enzymatic adaptation to allosteric transitions. *Science*, 154:475–483, 1966. [2](#)
- [56] J. Monod, J. Changeux, and F. Jacob. Allosteric proteins and cellular control systems. *Journal of Molecular Biology*, 6:306–329, 1963. [2](#)
- [57] J. Monod, J. Wyman, and J. Changeux. On the nature of allosteric transitions: a plausible model. *Journal of Molecular Biology*, 12:88–118, 1965. [2](#)
- [58] M. Morohashi, A. E. Winn, M. T. Borisuk, H. Bolouri, J. Doyle, and H. Kitano. Robustness as a measure of plausibility in models of biochemical networks. *Journal of Theoretical Biology*, 216:19–30, 2002. [8](#)
- [59] H. Motulsky and A. Christopoulos. *Fitting Models to Biological Data using Linear and Nonlinear Regression*. GraphPad PRISM, 2003. [54](#)
- [60] J. D. Murray. *Mathematical Biology: I. An Introduction*. Springer, 2002. [8](#)

- [61] D. Nevozhay, R. M. Adams, K. F. Murphy, K. Josic, and G. Balazsi. Negative autoregulation linearizes the dose-response and suppresses the heterogeneity of gene expression. *Proceedings of the National Academy of Sciences of USA*, 106:5123–5128, 2009. [17](#)
- [62] A. Novick and M. Weiner. Enzyme induction as an all-or-none phenomenon. *Proceedings of the National Academy of Sciences of USA*, 43:553–566, 1957. [1](#)
- [63] P. Nurse. A long twentieth century of the cell cycle and beyond. *Cell*, 100:71–78, 2000. [1](#)
- [64] K. Ogata. *Modern control engineering*. Prentice Hall, 2002. [3](#)
- [65] E. M. Ozbudak, M. Thattai, H. N. Lim, B. I. Shraiman, and A. Van Oudenaarden. Multistability in the lactose utilization network of *Escherichia coli*. *Nature*, 427:737–740, 2004. [5](#)
- [66] L. Pauling. The oxygen equilibrium of hemoglobin and its structural interpretation. *Proceedings of the National Academy of Sciences of USA*, 21:186–191, 1935. [2](#)
- [67] L. Perko. *Differential equations and dynamical systems*. Springer-Verlag, 2001. [2](#)
- [68] E. Plahte, T. Mestl, and S. W. Omholt. Feedback loops, stability and multistationarity in dynamical systems. *Journal of Biological Systems*, 3:409–413, 1995. [4](#)
- [69] A. Platt and R. J. Reece. The yeast galactose genetic switch is mediated by the formation of a gal4p-gal80p-gal3p complex. *The EMBO Journal*, 17:4086–4091, 1998. [47](#), [68](#)
- [70] S. A. Ramsey, J. J. Smith, D. Orrell, M. Marelli, T. W. Petersen, P. de Atauri, H. Bolouri, and J. D. Aitchison. Dual feedback loops in the *gal* regulon suppress cellular heterogeneity in yeast. *Nature Genetics*, 38:1082–1087, 2006. [47](#)
- [71] H. S. Rhee and B. F. Pugh. Comprehensive genome-wide protein-dna interactions detected at single-nucleotide resolution. *Cell*, 147:1408–1419, 2011. [58](#)
- [72] M. Santillan, M. C. Mackey, and E. S. Zeron. Origin of bistability in the *lac* operon. *Biophysical Journal*, 92:3830–3842, 2007. [5](#)

- [73] K. V. I. Saputra, L. van Veen, and G. R. W. Quispel. The saddle-node-transcritical bifurcation in a population model with constant rate harvesting. *Discrete and Continuous Dynamical Systems - Series B*, pages 233–250, 2010. [19](#)
- [74] M. Sedighi and A. M. Sengupta. Epigenetic chromatin silencing: bistability and front propagation. *Physical Biology*, 4:246–255, 2007. [5](#)
- [75] I. H. Segel. *Enzyme Kinetics: Behavior and Analysis of Rapid Equilibrium and Steady-State Enzyme Systems*. 1975. [35](#)
- [76] L. A. Segel. *Mathematical models in molecular and cellular biology*. Cambridge University Press, 1980. [35](#)
- [77] L. A. Segel and M. Slemrod. The quasi-steady-state assumption: A case study in perturbation. *Society for Industrial and Applied Mathematics*, 31:446–477, 1989. [6](#)
- [78] G. Shinar and M. Feinberg. Structural sources of robustness in biochemical reaction networks. *Science*, 327:1389–1391, 2010. [7](#)
- [79] C. Soule. Graphic requirements for multistationarity. *ComplexUs*, 1:123–133, 2003. [5](#)
- [80] M. Stamatakis and K. Zygorakis. Deterministic and stochastic population-level simulations of an artificial *lac* operon genetic network. *BMC Bioinformatics*, 12:301, 2011. [5](#)
- [81] J. Stelling, E. D. Gilles, and F. J. Doyle. Robustness properties of circadian clock architectures. *Proceedings of the National Academy of Sciences of USA*, 101:13210–13215, 2004. [8](#)
- [82] J. Stelling, U. Sauer, Z. Szallasi, F. J. Doyle, and J. Doyle. Robustness of cellular functions. *Cell*, 118:675–685, 2004. [8](#)
- [83] Z. Szallasi, J. Stelling, and V. Perival (editors). *System modeling in cellular biology: From concepts to nuts and bolts*. MIT Press, 2006. [1](#)
- [84] R. Thomas. On the relation between the logical structure of systems and their ability to generate multiple steady states or sustained oscillations. In J. Della-Dora, J. Demongeot, and B. Lacolle, editors. *Numerical methods in the study of critical phenomena, Springer Series in Synergetics*, 9:180–193, 1981. [4](#)

- [85] R. Thomas. The role of feedback circuits: Positive feedback circuits are a necessary condition for positive real eigenvalues of the jacobian matrix. *Berichte der Bunsengesellschaft fuer Physikalische Chemie*, 98:1148–1151, 1994. [4](#)
- [86] R. Thomas and M. Kaufman. Multistationarity, the basis of cell differentiation and memory. i. structural conditions of multistationarity and other nontrivial behavior. *Chaos*, 11:170–179, 2001. [4](#)
- [87] A. Tiwari and O. A. Igoshin. Coupling between feedback loops in autoregulatory networks affects bistability range, open-loop gain and switching times. *Physical Biology*, 9:055003, 2012. [17](#)
- [88] L. Trotta, E. Bullinger, and R. Sepulchre. Global analysis of dynamical decision-making models through local computation around the hidden saddle. *PLoS ONE*, 7:e33110, 2012. [8](#), [29](#), [34](#)
- [89] T. Turanyi. Sensitivity analysis of complex kinetic systems. tools and applications. *Journal of Mathematical Chemistry*, 5:203–248, 1990. [11](#)
- [90] J. J. Tyson and B. Novak. Irreversible transitions, bistability and checkpoint controls in the eukaryotic cell cycle: a systems-level understanding. In *A.J. Marian Walkout, Marc Vidal and Job Dekker, editors. Handbook of Systems Biology. Elsevier, San Diego CA*, pages 265–285, 2012. [5](#)
- [91] H. E. Umbarger. Feedback control by end product inhibition. *Cold Spring Harbor Symposia on Quantitative Biology*, 26:301–312, 1961. [1](#)
- [92] C. Venter. Computing 2010: from black holes to biology. *Nature*, 402:C67–C70, 1999. [1](#)
- [93] O. S. Venturelli, H. El-Samad, and R. M. Murray. Synergistic dual positive feedback loops established by molecular sequestration generate robust bimodal response. *Proceedings of the National Academy of Sciences of USA*, 109:3324–3333, 2012. [5](#), [47](#), [59](#)
- [94] A. Verdugo, P. K. Vinod, J. J. Tyson, and B. Novak. Molecular mechanisms creating bistable switches at cell cycle transitions. *Open Biology*, 3:120179, 2013. [5](#)
- [95] E. O. Voit. *Computational Analysis of Biochemical Systems: A Practical Guide for Biochemists and Molecular Biologists*. Cambridge University Press, 2000. [11](#)

BIBLIOGRAPHY

- [96] V. Volterra. *Lecons sur la Theorie Mathematique de la Lutte pour la Vie*. Paris, France: Gauthier-Villars, 1931. [1](#)
- [97] C. H. Waddington. *The strategy of the genes. A discussion of some aspects of theoretical biology*. George Allen & Unwin Ltd, 1975. [1](#)
- [98] S. Wiggins. *Introduction to applied nonlinear dynamical systems and chaos*. Springer-Verlag, 2003. [2](#)
- [99] J. Zhang, Z. Yuan, H. Li, and T. Zhou. Architecture-dependent robustness and bistability in a class of genetic circuits. *Biophysical Journal*, 99:1034–1042, 2010. [8](#)
- [100] Q. Zhang, S. Bhattacharya, and M. E. Andersen. Ultrasensitive response motifs: basic amplifiers in molecular signaling networks. *Open Biology*, 3: 130031, 2013. [3](#)

Amirhossein Hajhosseini

Personal Data

PLACE AND DATE OF BIRTH: Tehran, Iran | 29.12.1980

FAMILY STATUS: Married | No Children

CONTACT: +41 77 4622271 | amirhossein80@gmail.com

Education

| | |
|----------|--|
| JAN 2012 | Ph.D. in Systems Biology |
| DEC 2015 | Biozentrum, University of Basel, Basel, Switzerland |
| SEP 2005 | M.Sc. in Applied Mathematics |
| SEP 2007 | School of Mathematics, Statistics and Computer Science University of Tehran, Tehran, Iran |
| SEP 1999 | B.Sc. in Applied Mathematics |
| AUG 2003 | Department of Mathematics, Shahed University, Tehran, Iran |

Professional Experience

| | |
|----------|--|
| SEP 2013 | Teaching Assistant |
| SEP 2015 | Biozentrum, University of Basel, Basel, Switzerland |
| JAN 2007 | Researcher |
| JAN 2012 | Center of Excellence in Biomathematics University of Tehran, Tehran, Iran |
| JUN 2010 | Research Assistant |
| JAN 2012 | School of Mathematics Institute for Research in Fundamental Sciences (IPM), Tehran, Iran |

| | |
|----------|--|
| JUN 2008 | Research Collaborator |
| SEP 2009 | School of Pharmacy Tehran University of Medical Sciences (TUMS), Tehran, Iran |
| FEB 2006 | Teaching Assistant |
| DEC 2008 | School of Mathematics, Statistics and Computer Science University of Tehran, Tehran, Iran |
| SEP 2003 | Private Math and Physics Tutor |
| SEP 2005 | |

Publications

1. I. Majer, **A. Hajhosseini**, A. Becskei. *Identification of optimal parameter combinations for the emergence of bistability*. *Physical Biology* **12** (2015) 066011.
2. G. R. Rokni Lamooki, F. Maleki, **A. Hajhosseini**. *A mathematical model for the ICU admission process*. *Communications in Nonlinear Science and Numerical Simulation* **19** (2014) 8-18.
3. **A. Hajhosseini**, F. Maleki, G. R. Rokni Lamooki. *Bifurcation analysis on a generalized recurrent neural network with two interconnected three-neuron components*. *Chaos, Solitons & Fractals* **44** (2011) 1004-1019.
4. Z. Zamani, **A. Hajhosseini**, A. Masoudi-Nejad. *Computational Methodologies for Analyzing, Modeling and Controlling Gene Regulatory Networks*. *Biomedical Engineering and Computational Biology* **2** (2010) 47-62.
5. F. Maleki, B. Beheshti, **A. Hajhosseini**, G. R. Rokni Lamooki. *The Bogdanov-Takens bifurcation analysis on a three dimensional recurrent neural network*. *Neurocomputing* **73** (2010) 3066-3078.
6. **A. Hajhosseini**, G. R. Rokni Lamooki, B. Beheshti, F. Maleki. *The Hopf bifurcation analysis on a time-delayed recurrent neural network in the frequency domain*. *Neurocomputing* **73** (2010) 991-1005.
7. **A. Hajhosseini**, G. R. Rokni Lamooki. *Bifurcation analysis on the FitzHugh-Nagumo Neural Model*. *Dynamics of Continuous, Discrete and Impulsive Systems, Series A: Mathematical Analysis* **17** (2010) 233-248.